國立交通大學

光電工程學系　光電工程研究所

碩士論文

利用介電層表面處理提升負型有機薄膜電晶體
在大氣下之穩定性

Improved air-stability of n-channel organic thin-film transistors with surface modification on gate dielectrics

研究生：廖呈祥

指導教授：陳方中　博士

中華民國九十七年七月

利用介電層表面處理提升負型有機薄膜電晶體
在大氣下之穩定性

Improved air-stability of n-channel organicthin-film transistors with surface modification on gate dielectrics

研 究 生：廖呈祥　　　　　　　Student：Cheng-Hsiang Liao

指導教授：陳方中 博士　　　　　Advisor：Dr. Fang-Chung Chen

國 立 交 通 大 學
電機學院光電工程研究所碩士班
碩 士 論 文

A Thesis
Submitted to Institute of Electro-Optical Engineering
College of Electrical and Computer Engineering
National Chiao Tung University
In Partial Fulfillment of the Requirements
For the Degree of Master
In
Electro-Optical Engineering
July 2008
Hsinchu, Taiwan, Republic of China

中華民國九十七年七月

利用介電層表面處理提升負型有機薄膜電晶體在大氣下之穩定性

學生：廖呈祥　　　　　　　　　指導教授：陳方中

國立交通大學光電工程研究所碩士班

中文摘要

　　本研究選用不同高分子介電材料，將其塗佈於二氧化矽的絕緣層表面，研究不同高分子修飾層對負型有機電晶體元件特性之影響，特別針對元件於一般大氣下之穩定性做深入的探討。由實驗結果發現選擇適當的高分子修飾層能夠有效的提高元件效能並且表現出較好的穩定性。我們知道在一般的二氧化矽表面上會有很多SiOH鍵結，這些鍵結往往對於負型有機電晶體有抑制其元件電性的效果，容易於介電層表面產生SiO⁻等官能基而局限電子。疏水性強的高分子材料能夠有效的減少在二氧化矽表面上的電子陷阱(SiO⁻)，並且可以由原子力顯微鏡與X光晶格繞射圖譜等分析結果發現這些高疏水性的表面能夠使有機半導體分子有更好的晶格排列性，進而提高負型電晶體之元件特性與穩定性。

Improved air-stability of n-channel organicthin-film transistors with surface modification on gate dielectrics

Student: Cheng-Hsiang Liao   Advisor: Dr. Fang-Chung Chen

Institute of Electro-Optical Engineering
National Chiao Tung University

Abstract

Improved air-stability of n-channel organic thin film transistors using N,N'-dioctyl-3,4,9,10-perylene tetracarboxylic diimide as the active material has been demonstrated by modifying the dielectric surfaces with various polymer insulators. The appropriate polymer dielectric plays an important role in the n-channel conduction for organic transistors. The hydrophobic nature of the polymer surfaces inhibits the protonation reaction of siloxyl groups on the SiO_2 surface, leading to less SiO^- groups, which could behave as electron trapping sites. Additionally, the hydrophobic polymer surface can also enhance the crystallinity of PTCDI-C8 thereby improving the transfer characteristics. Among the polymer insulators, the device modified with hydroxyl-free polymers exhibited better air-stability. Overall, the improved stability is attributed to the passivation of the electron trapping sites on the dielectric surfaces.

誌謝

感謝主，一切有祢的看顧，讓我平安順利地完成學業。碩士生涯即將告一段落，回想這兩年來的一切，看似匆匆的走過，卻也留下了許多值得細細品味的回憶。這段日子裡，無論在實驗研究的領域或是日常生活上的人際互動，很慶幸能得到許多人的幫助，令我獲益良多。

首先，由衷地感謝指導教授陳方中博士，在我的研究生涯當中時常給予關鍵的指導，在我困惑的時候總是能拉我一把，給予信心，使我得以突破研究上的困境。除此之外，對於日常生活上的叮嚀更是深刻的教誨，相信這兩年裡所獲得的遠大於論文中所提及的，這些收穫在未來必定能有所受用。

接著，感謝實驗室博士班的學長，文奎、祖榮、喬舜、志平學長將寶貴的知識觀念毫不保留地細心傳授教導，特別感謝喬舜學長對於我的實驗研究上的指點，時常教導我從不同的觀點來看一個問題，不只增廣見聞也總是能夠獲得研究上的幫助。也要感謝過去曾經給予指教的學長姐，永昇、立仁、文生、瑞祥、惠君，以及泰元、映頻、上傑、義凱、浩偉、志力、紓婷、尹婷，由於有學長姐的帶領與悉心指導，讓我在短時間進入研究與實驗的狀態，並且時時給予鼓勵讓我更有信心完成這份研究，很慶幸我選擇了這間充滿親切氣氛的實驗室。

朝夕相處的夥伴們，昱仁、政豪、永軒、煒棋、太獅、信展、曉芬，因為有你們，實驗室更添許多歡樂的氣份，懷念那一起打球玩樂的時光，也有你們的相互扶持協助，讓每個人都得以順利完成自己的研究生涯。實驗室的學弟妹，威寬、炳瑞、冠霖、佳霖、洪毅、文哲，感謝你們在實驗室的幫忙，讓我能心無旁騖地專心於自己的實驗上。

還要給我最麻吉的 416-311 室友們：小毛、白虎、鴕鳥、小日本、小垂垂，你們不只是我最要好的大學同學，也是我在寢室裡最忠實的聽眾，讓我在研究之餘找到另一個舒壓的出口，聽到你們的笑聲對我來說就是最棒的娛樂，由衷地感謝你們，也祝福大家在畢業之後都有不錯的發展並且擁有各自的一片天。

最後，特別要感謝我最親愛的阿公(水旺)、父母(顯彬、碧雲)還有我的兩位姊姊和妹妹(玉婷、玉琪、玉涵)，不時給我打氣和鼓勵讓我有所依靠；也感謝我的女友(冠伶)，願意當我的垃圾桶，並且時時給予安慰與支持，因為你們讓我更有信心地致力於研究，再多的言語也道不盡我對你們的感激，僅以此文獻給我由衷感謝的人，謝謝你們。

Contents

List of Tables

Figure Captions

Chapter 1

Chapter 2

Chapter 3

Chapter 4

Chapter 1
Introduction

1.1 Preface

Organic thin-film transistors (OTFTs) have received much attention from many researchers and scientists because of their potentially mechanical flexibility. Moreover, they could serve as the main component in low-cost, flexible and large-area electronic circuits. To date, there are many potential applications have been proposed, such as flexible displays[1,2] and radio frequency identification (RF-ID) tags[3-7] (Figure 1.1 and 1.2). Organic semiconductors have been known since the late 1940s.[8] Scientifically, organic semiconductors show interesting characteristics both similar to and different from known inorganic semiconductors, especially amorphous silicon.
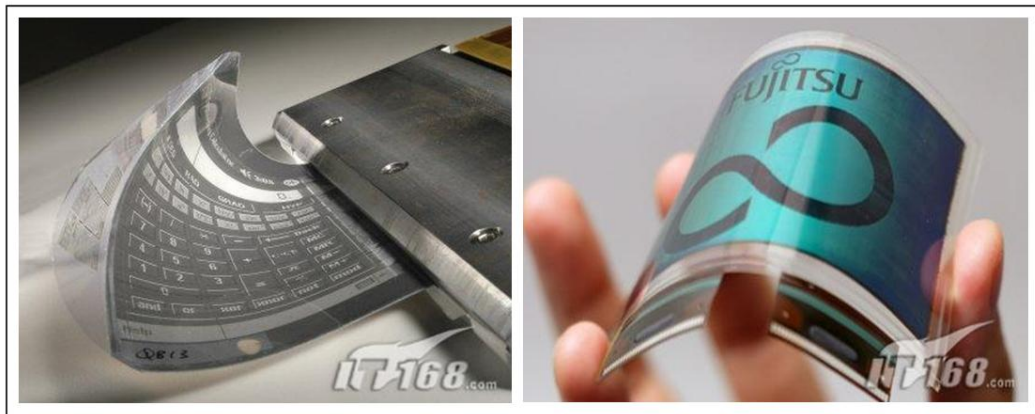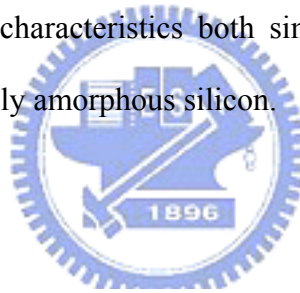
Figure 1. 1 The application of plastic transistors: flexible displays.

[Adapted from http://tech.sina.com.cn/digi/2006-04-20/1204911539.shtml]
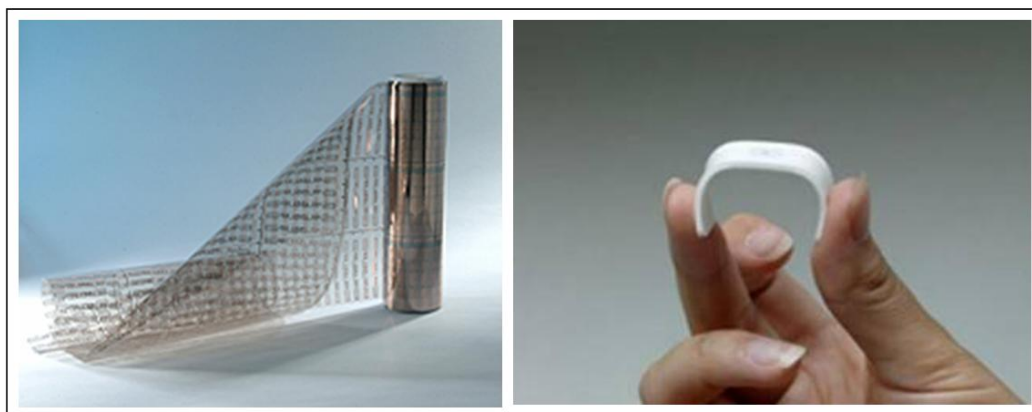
Figure 1. 2   The application of plastic transistors: radio frequency identification (RF-ID) tags.

[Left one is adapted from www.patent-cn.com/2007/10/17/6247.shtml]
[Right one is adapted from http://www.hanitacoatings.com/products/copper_rfid.asp]

Many of these OTFTs exhibit p-channel while a negative gate voltage is applied. However, when reversely positive bias voltage is applied on gate, the formation of an electron-accumulated channel is rarely observed. Typical p-channel organic semiconducting materials are shown in Figure 1.3. Over the last six years, many groups have made efforts in realizing "n-channel" thin-film transistors. The active organic materials usually involved complicated chemical synthesis to realize high electron affinities. The most common approach is to attach strong electron withdrawing groups on the active moities. These are usually called "n-channel" organic semiconductors as shown in Figure 1.4.[9]
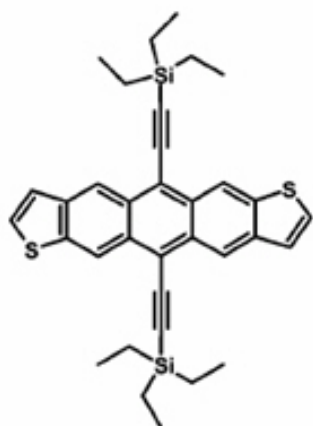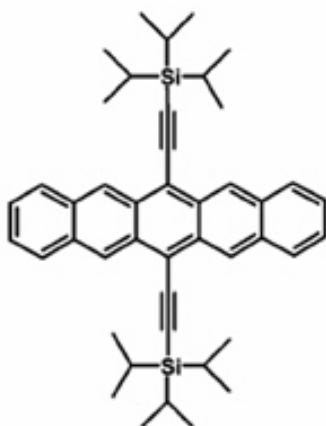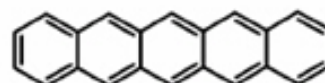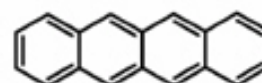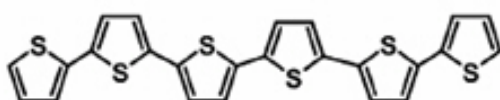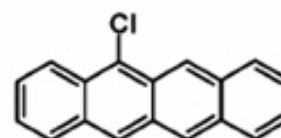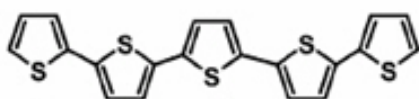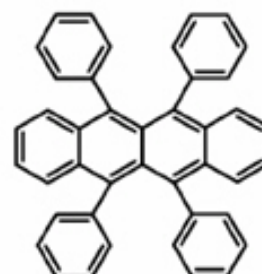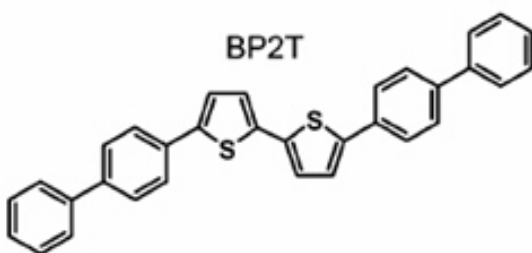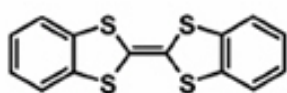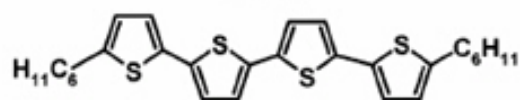
Figure 1. 3 P-type organic semiconductor materials.[9]
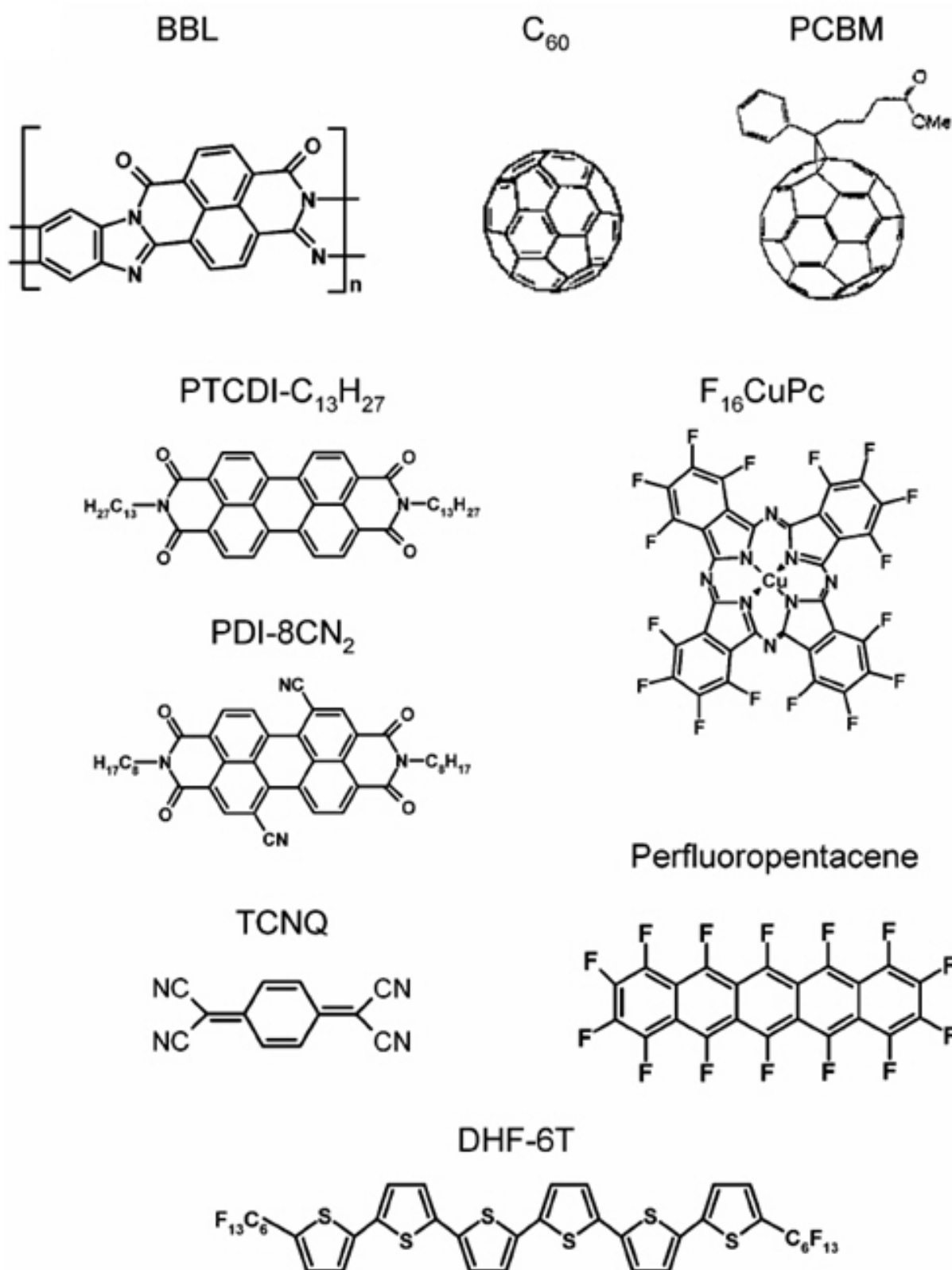
Figure 1. 4 N-type organic semiconductor materials.[9]

High performance of p-channel organic thin-film transistors (OTFTs) comparable to that of amorphous silicon have been achieved.[9] For example, a hole mobility higher than 1 $cm^2V^{-1}s^{-1}$ has been demonstrated for devices based on pentacene.[10,11] Compared with organic p-channel material, the stability and performance of the n-channel material are relatively poor. Moreover, for the development of electronic circuits based on organic semiconductors, the electronic characteristics of n-channel TFTs must match that of p-channel transistors. Therefore, n-channel TFTs play an important role in electronic circuits.

1.2 View of N-channel Organic Thin-Film Transistors

For p-type transistors, the highest occupied molecular orbital (HOMO) level of many organic semiconductors is in the range of 4.8 to 5.3 eV. Therefore, one can easily use gold electrodes (the work function of gold is about 5.2 eV) to achieve efficient injection of holes into the HOMO level of organic semiconductors. On the other hand, for high performance n-channel OTFTs, electrons must inject efficiently into the lowest unoccupied molecular orbital (LUMO) of organic materials. The LUMO level of organic semiconductors is often much lower (around 2~3 eV). To match the LUMO level, we need to use low work function metals, such as calcium, magnesium, or aluminum; nevertheless, these materials are not stable under ambient environment.

The second obstacle to realized n-channel OTFTs is the susceptibility of n-type organic semiconductors to water and oxygen under ambient atmosphere. Thus many n-type transistors can only be operated when processed and tested under inert conditions excluding oxygen and water.[12,13] When a positive gate voltage is applied, the organic radical anions are present in the channel. These radical anions have a very high reducing power and can react easily with water or oxygen that have diffused into the organic film.[9] How to find out several effective methods to solve the problem has became an interesting investigative aspect.

1.3 Motivation

Although high performance n-channel devices have been reported, most of them could be only observed under inert atmosphere.[13-18] The atmospheric O_2 and H_2O have been suggested as the main oxidants and/or electron traps responsible for n-channel degradation under ambient conditions.[9,14] The most successful approach for ambient stable n-channel OTFTs is to synthesis organic compounds with strong electron-withdrawing groups, such as -CN, and –F, as the semiconducting materials.[12,19-22] Such electron-withdrawing side chains probably lead to a high electron affinity, stabilizing the charge carriers, and improve the close packing of the molecules that prevents the diffusion of O_2 and H_2O into the conducting channel.[9] However, although this method is very promising, complicated chemical synthesis is necessarily required.

Therefore, people need to find out another simple method other than those involving complicated chemical synthesis to achieve air-stable n-channel OTFTs. To established n-type OTFTs, we chose N,N'-dioctyl-3,4,9,10-perylene tetracarboxylic diimide (PTCDI-C8) as the semiconducting material. Perylene diimide, frequently reported in resent years, exhibits excellent n-channel behavior, which could attribute to the relatively large electron affinity assisting the electrons accumulation of electrons on the interface between the semiconductor layer and the dielectric layer. Further, it has large π-stacks that could enhance charge hoping through the intermolecular π-orbital overlapping.[15,16,20,23] In this work, substantially improved air-stability of n-channel OTFTs based on N,N'-dioctyl-3,4,9,10-perylene tetracarboxylic diimide (PTCDI-C8), which is not considered as an air-stable n-channel organic compound, is obtained by modifying the dielectric surface with insulating polymers. In addition, the electrical field-effect mechanism on n-type organic transistors with various insulating polymer materials is also discussed.

1.4 Thesis Organization

This thesis is organized as following. In this chapter, the background of this study is described briefly; and in the following chapter, we have introduced the basic knowledge about field-effect transistors and organic crystals. The useful tools of analysis are also presented in this part. The experimental details are shown in the third chapter and the procedures of the organization of OTFTs are illustrated including surface treatments and thin-film deposition. Apart from the device fabrication, the analysis methods are also particularly taken into account. In chapter 4, there are discussions for devices with different surface modification. Further, the surface states of polymer dielectric layer and organic semiconductor were investigated by using atomic force microscopy (AFM), contact angle (CA) measurement, and X-ray diffraction techniques. In addition, we also conducted two experiments to expound our conjecturing mechanisms in this chapter. Finally, conclusions are remarked in the last chapter.

Chapter 2
Review and Principles

2.1 The Charge Carrier Transportation in Organic Semiconductors

The interaction between molecules in solid-state organic materials is van der Waals force, which is relatively weaker than the covalent bonding between the atoms in inorganic materials. Hence the mechanism of charge carrier transportation is quite different between organic and inorganic materials.

The π-bonding electron cloud has two states: localized states and delocalized states. The π-bonding electron is localized if the electron is bounded to particular atom. The localized π-bonding electron can not be contributed to the carrier transportation. Figure 2.1 shows the π-bonding electron states of benzene.

Generally, there are two models to describe the delocalized electrons transportation in organic materials, which are "hopping model"[24] and "multiple trapping and release model" (MTR)[25] described in the following subsections.
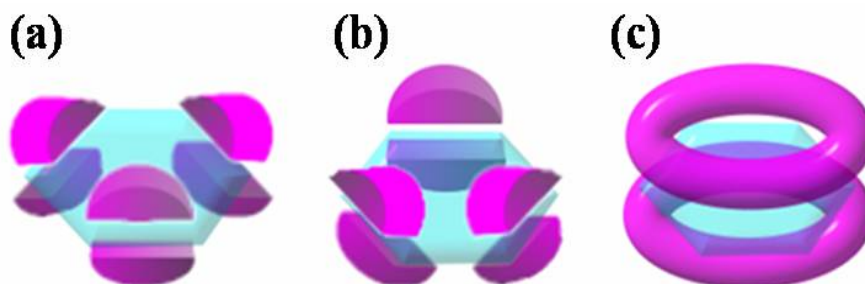
Figure 2. 1   electron states (a), (b): localized states; (c): delocalized states.

2.1.1 Hopping Model
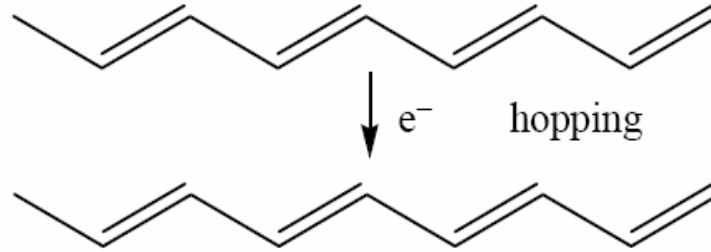
Figure 2. 2 Charge carrier hopping.[24]

In organic materials, the intermolecular transportation of charge carrier depends on hopping as shown in Figure 2.2. This is the limitation of the charge carrier mobility in organic materials. Because the phonons would assist the hopping of carriers, the mobility increases with the increasing temperature. The relation between the mobility of the hopping and the temperature can be described as the following equation: $\mu = \mu_0 \exp[-(T_0 / T)^{1/\alpha}]$ where the α is ranged from 1 to 4.

2.1.2 Multiple Trapping and Release (MTR)

The MTR model is widely used in the physical mechanism of amorphous silicon semiconductors, in which it assumes that there are localized levels in the band gap caused by the defect states. These localized levels are like traps for charge carriers. These levels would form a narrow band with high concentration of trap levels. When the charge carriers transport to the levels, the carriers would be trapped with the probability near 100%. On the other hand, the activation energy of the carrier determines the release of the carrier. The released carrier would contribute to the transportation and the drift mobility is given as following:

$$\mu_D = \mu_0 \alpha \exp(-E_t / kT)$$

where E_t is the energy level of the defects, α is the ratio between the density of states at the bottom of the band and the density of traps.[25]

2.2 The Structures of OTFTs

The bottom-contact OTFTs and top-contact OTFTs, as shown in Figure 2.3, are the two most common device structure of OTFTs so far. However, the device characteristics are usually different. Most studies are focused on top contact configuration, in which the source-drain contacts are patterned by shadow masking on top of the organic semiconductor, because of its better and stable performance [Figure 2.3(a)]. Unfortunately, this process cannot be used for devices with smaller sizes. On the other hand, Figure 2.3(b) shows the bottom contact structure in which this fabrication process can be conducted in coordination to common inorganic semiconductor process with ultra-short channel length and improved electrode patterns by the photolithograph technology.
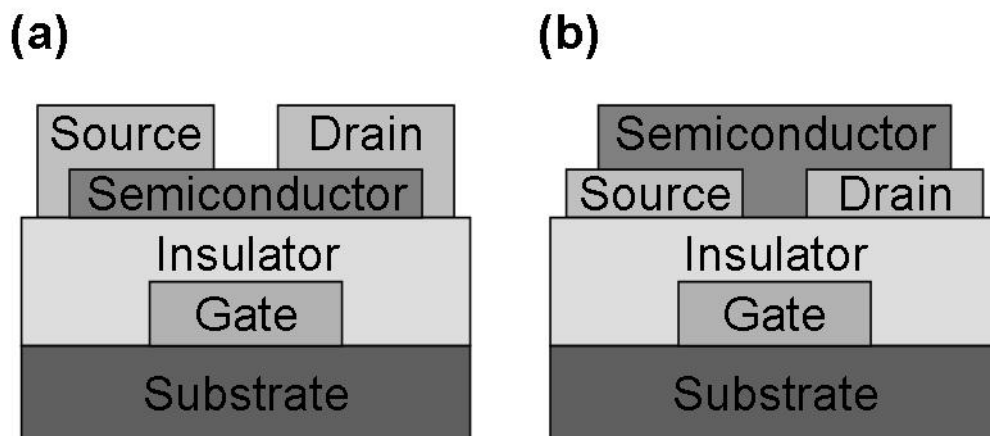
Figure 2. 3 The basic structures of OTFTs: (a) Top-contact device, (b) Bottom-contact device.

The advantage of top contact structures is the smaller contact resistance exhibited between the active layer and electrodes and the performance is generally better, but the channel length defined by shadow masks is hardly decreased. The OTFTs with top contact structures have relative high off current because the back-channel currents flow near the source-drain electrodes. On the contrary, the OTFTs with bottom-contact structures have relative low off current. Because the active layer is deposited on source and drain electrodes, the contact between the organic semiconductors and source-drain electrodes in the channel region is poor, hence high contact resistance and worse performance are presented.

2.3 The Operation of Organic FETs

In n-channel silicon MOSFETs, the source and drain terminations are heavily n-doped and the bulk semiconductor is p-doped. The transistor is initially in "OFF" state without gate bias. When a positive gate voltage bias is applied, the holes near the semiconductor/insulator interface are repelled and the electrons start to accumulate thus forming a channel between the source and drain electrodes. This transistor is operated in inversion mode.

On the other hand, the organic thin-film transistors are usually operated in accumulation mode. The holes would accumulate in the interface between the active layer and the insulator since the gate is biased at a negative voltage. When a transistor is operated in "ON" state, there are enough holes accumulated in the interface and then the conducted channel is formed. While a negative voltage is applied at the drain electrode, the current would flow from the source to drain electrode. Figure 2.4 illustrates the operation of the p-channel and n-channel organic transistors. For a positive gate voltage, negative charges (electrons) would be induced at the interface between active layer and insulator, and then that were injected from the source electrode.
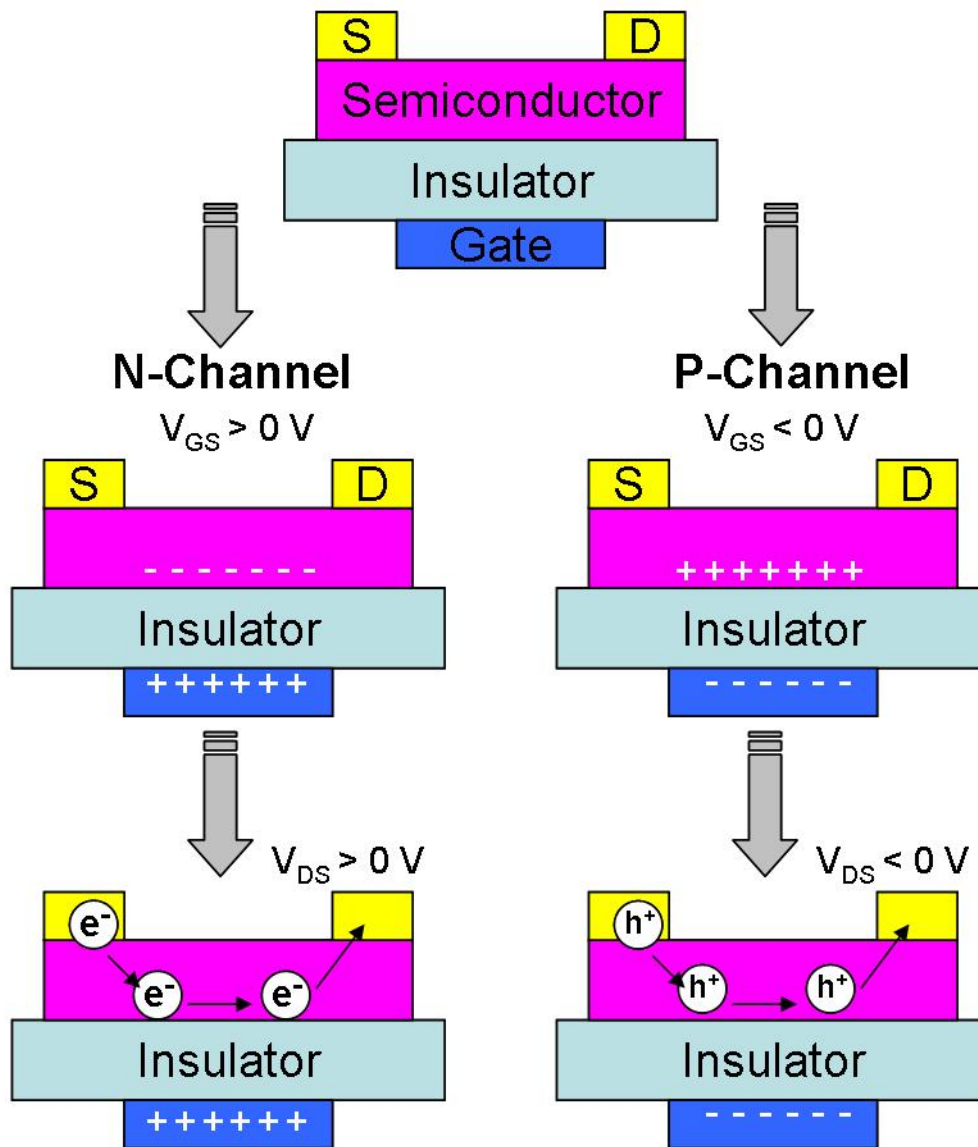
Figure 2. 4 The operation of p-type and n-type organic thin-film transistors.[9]

The collections of charges accumulated in the active layer are proportional to the date bias and the capacitance of the insulator. Take notice of interfacial states, the deep traps have to be filled firstly before the additionally induced charges become mobile. Even though the immobile charged carriers are obtained in trap states, the other mobile charges will thus contribute to the current in a field-effect transistor. Particularly, the gate voltage is

must biased more highly than the threshold voltage since $V_{GS} - V_{Th}$ is the effective driving voltage to accumulate more mobile charged carriers. The interfacial dipoles can generally create an internal potential at the semiconductor interface upon the insulator at zero gate bias and thus cause accumulation of additional charges (mobile or immobile) in the channel so that a obvious turn-on voltage shift is exhibited in the transfer characteristics.[26,27]
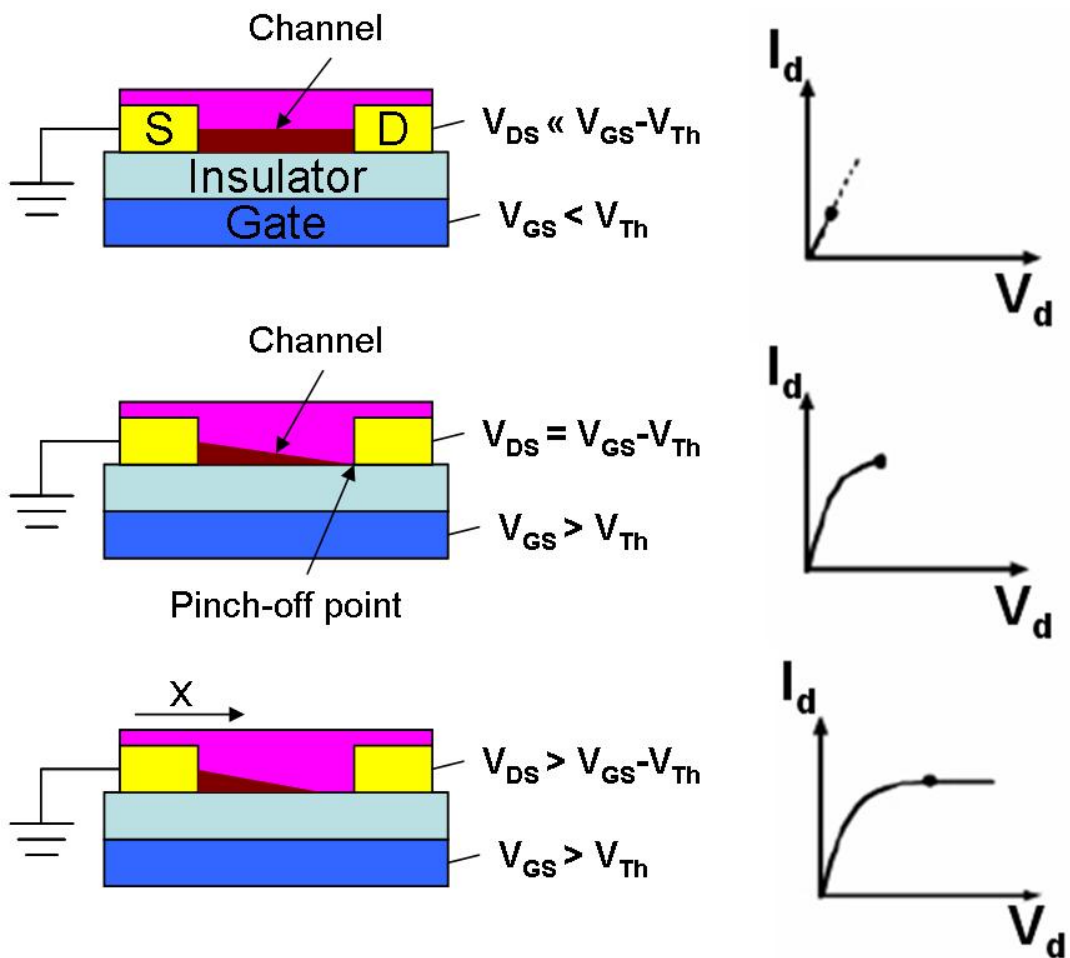
Figure 2. 5 The basic operating regimes and associated current-voltage characteristics of organic field-effect transistors.[9]

The following illustrates the basic operating modes and associated current-voltage characteristics of a field-effect transistor (Figure 2.5). Without applied source-drain bias, the

charge carrier concentration in the transistor channel is uniform. A linear gradient of charge density from the carrier-injecting source to the extracting drain forms when a small source-drain voltage is applied. In the linear regime, the current flowing through the channel in the active layer is directly proportional to drain-to-source bias. The potential $V(x)$ within the channel increases linearly from the source $[V_{(x = 0)} = 0 \text{ V}]$ to the drain electrode $[V_{(x = L)} = V_{DS}]$. The pinched-off point is obtained when the drain-to-source voltage is further increased to a point of $V_{DS} = V_G - V_{Th}$.

That means a depletion region forms next to the drain because the difference between the local potential $V(x)$ and the gate voltage is now below the threshold voltage. A space-charge-limited saturation current $I_{ds,sat}$ can flow across this narrow depletion zone as carriers are swept from the pinch-off point to the drain by the comparatively high electric field in the depletion region.

Eventually, increasing the drain-to-source voltage will not substantially increase the drain current but leads to an expansion of the depletion region in the channel region, and thus a slight shortening of the channel will be obtained. Since the potential at the pinch-off point remains $V_{GS} - V_{Th}$ and thus the potential drop between that point and the source electrode stays approximately the same, the current saturates at a level $I_{ds,sat}$. In the following section, we will introduce principal parameters extraction of OTFTs from their electrical characteristics.

2.4 The Parameters Extraction of Organic Thin Film Transistors

The transistor is a three-terminal device and there are two transfer characteristics plots. The first plot is I_D-V_D characteristics as shown in Figure 2.6. The I_D versus V_D relation is measured under several constant V_G. The I_D-V_D transfer characteristics are separated into two modes which are the linear and saturation modes. The linear mode occurs when the drain voltage of V_D is smaller than the bias of $V_{GS} - V_{Th}$, and the transistor behaves as a

resistance. When the drain voltage is applied more largely than V_{GS} - V_{Th}, the transistor is exhibited in saturation mode. In saturation mode, the drain current is determined by the gate bias. The second plot is I_D-V_G transfer characteristics as shown in Figure 2.7. From the I_D-V_G plot, many parameters like the mobility and threshold voltage can be extracted. The OTFTs are adequately modeled by standard field-effect transistor equations, as shown previously for other organic TFTs.[28,29] Although the transportation mechanism in organic materials is different from that of inorganic materials, the transfer characteristics are similar. The formula derived from the inorganic semiconductors was adopted to calculate the parameters like the field-effect mobility and threshold voltage in this study.
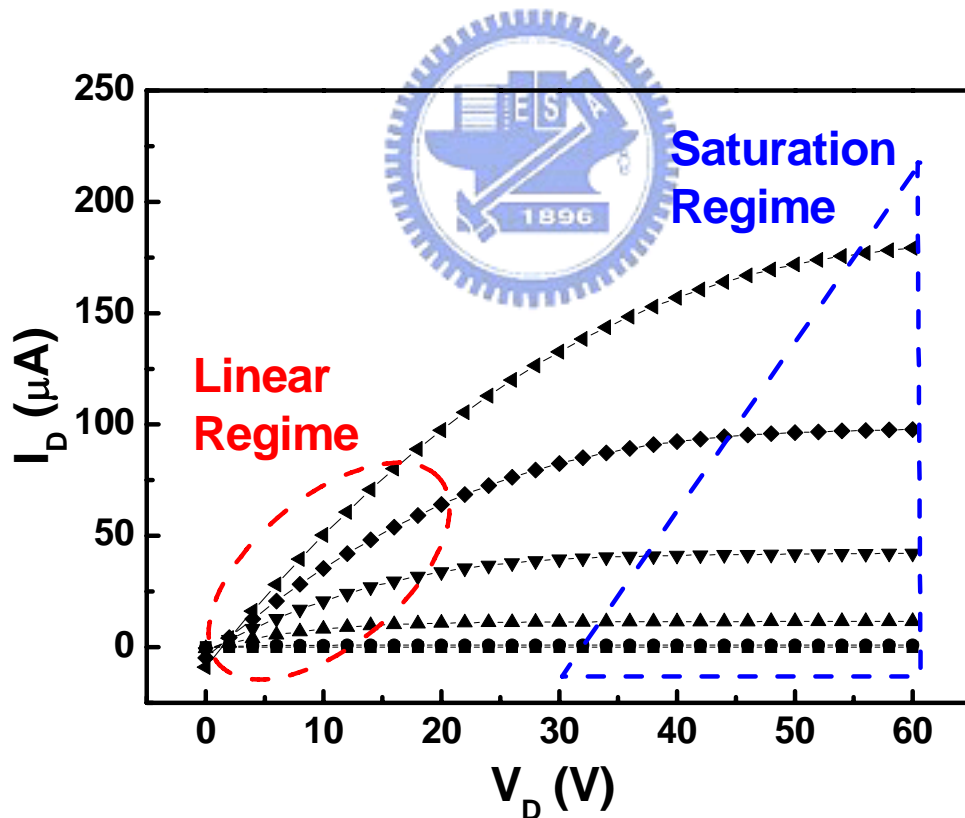
Figure 2. 6   The I_D-V_D output characteristics plot of the n-type transistor.

The typical n-channel I_D-V_D transfer characteristics are shown in Figure 2.6. When the TFT is operated at linear mode, the drain current is governed by the equation 2-1.

$$I_D = \frac{WC_i}{L} \mu (V_G - V_T - \frac{V_D}{2}) V_D \qquad (2\text{-}1)$$

where W is the channel width in cm, L is the channel length in cm, C_i is the capacitance per unit area in F/cm^2, μ is the field-effect mobility in cm^2/Vs, the V_T is the threshold voltage in Volt.

When $V_D > V_G - V_T$, the TFT is operated at saturation mode. The drain current is given by the equation 2-2.

$$I_D = \frac{WC_i}{2L} \mu (V_G - V_T)^2 \qquad (2\text{-}2)$$

The mobility μ can be calculated by differentiating the square root of I_D in saturation mode.

$$\left(\frac{\partial \sqrt{|I_D|}}{\partial V_G} \right)_{V_D = const} = \sqrt{\frac{WC_i}{2L} \mu} \qquad (2\text{-}3)$$

The slope can be obtained from the I_D-V_G transfer characteristics plot shown in Figure 2.7. One linear line is extracted by the square root of I_D in the $I_D^{1/2}$-V_G plot in the saturation regime, and the intersected point of the line and x-axis is defined as the threshold voltage (V_T). The turn-on voltage (V_{on}) and the on/off ratio can be obtained form the I_D-V_G transfer characteristics plot.

The subthreshold swing (S.S.) is a parameter to determine the switch speed of a transistor. It can be calculated by equation 2-4.

$$\text{S.S.} = \text{Min} \left[\left(\frac{\partial \log(|I_D|)}{\partial V_G} \right)^{-1}_{V_D = const} \right] \qquad (2\text{-}4)$$

The dimension of subthreshold swing is V/decade. The subthreshold swing gives the degree of the switch property of a transistor.
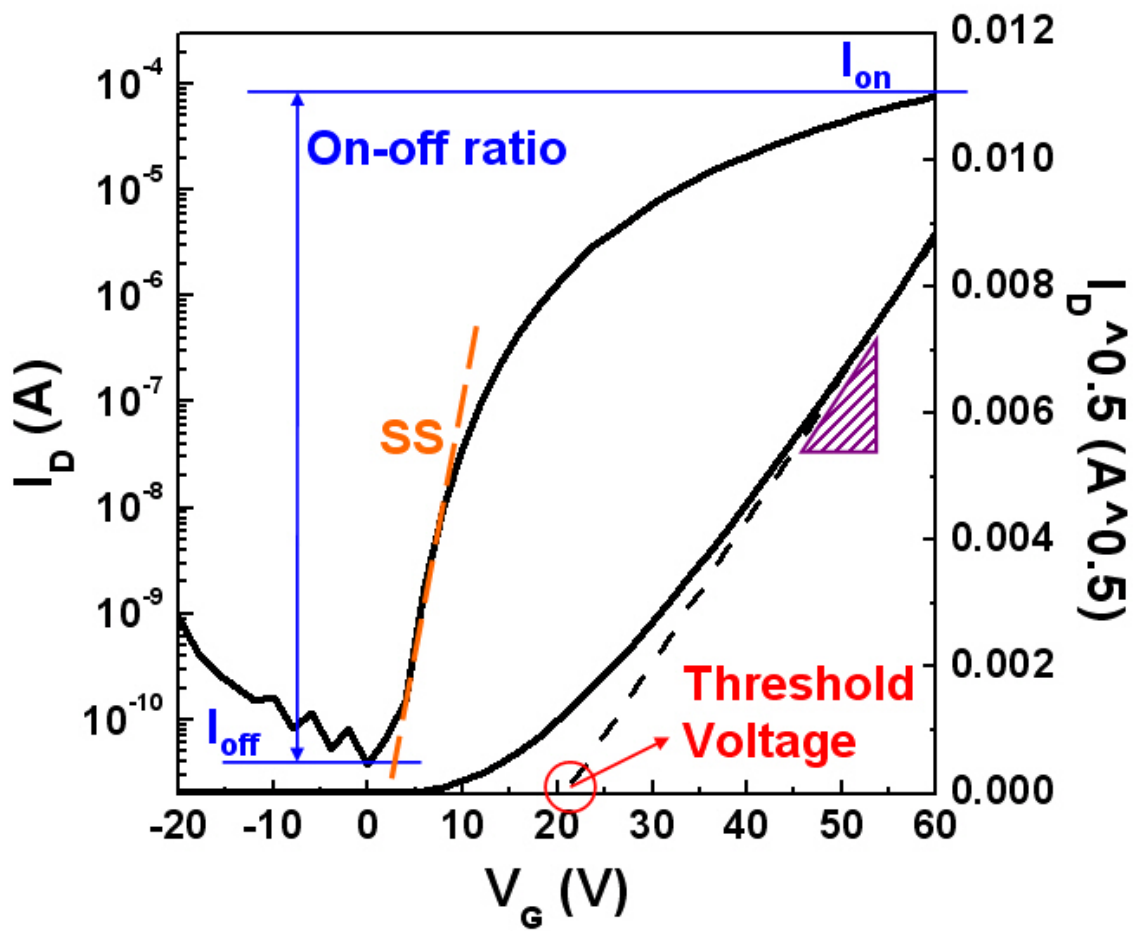
Figure 2. 7   The I_D-V_G transfer characteristics plot of the n-type transistor.

Chapter 3
Experiment

3.1 Device Fabrication

In the first section of this chapter, the procedures of device fabrication will be introduced. Particularly, each step of the processes would be described by indicating figures to recognize the device configuration formation. The top-contact structure was chosen to fabricate the n-channel OTFTs in our work and that reasons were illustrated previously in section 2.2. We preferred the contact among organic semiconductor and source-drain electrodes in top-contact structure because evaporative metals had higher kinetic energy to diffuse into the defects of organic surface, and thus the phenomenon can reduce the contact resistance in OTFTs fabrication. On the other hand, the metal surface was not a suitable environment for the growth of organic materials in bottom-contact structure.

In the following, the technological processes of OTFTs fabrication based on N,N'-dioctyl-3,4,9,10-perylene tetracarboxylic diimide (PTCDI-C8) would be illustrated clearly.

3.1.1 Preparation of Substrates

In this study, we use the heavily doped n-type silicon wafer, served as a gate electrode, with thermal SiO_2 to fabricate the substrates of experimental devices. The 200 nm-thick SiO_2 grown on the polished side of the wafer was served as the gate dielectric. The sheet resistance was about 0.001~0.003 ohm-cm and the measured capacitance per unit area is about 14.2 nF/cm^2.

3.1.2 Process of Cleaning SiO₂ Surface

The substrates, kept in a Teflon container, were subsequently cleaned by the prior steps of RCA process where we only used deionized water and 3:1 mixture of concentrated H_2SO_4 and H_2O_2. The details of procedure are illustrated in the following and the indicator is showed in Figure 3.1. After the procedures of substrate cleaning, the wafers were placed into an oven in which the temperature was set to 120℃ for over night to remove the water.
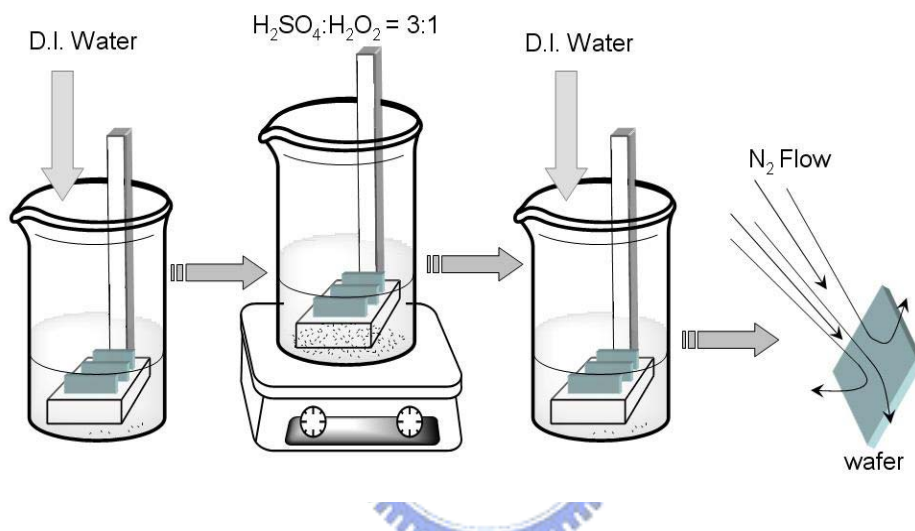
Figure 3. 1   The process of substrates cleaning.

● **The process of substrates cleaning:**

Step 1: Place the wafers on the Teflon container, and pre-rinse the wafers in the deionized water for 5 minutes.

Step 2: Submerge the Teflon container with wafers in the 3:1 mixture of concentrated H_2SO_4 and H_2O_2, and keep the temperature at 85℃ for 20 minutes.

Step 3: Remove the Teflon container from the acidic bath, and rinse it again in the deionized water for 5 minutes.

Step 4: Blow the wafers dry with nitrogen flow.

3.1.3 Surface Treatment

There were five different polymer dielectrics as shown in Figure 3.2 prepared in our work. The first one was bare SiO_2 dielectric surface without any modification, and the other four substrates were modified with different polymer dielectric materials on SiO_2 insulator by solution process. The following is the procedure of surface treatment with polymer dielectric materials.
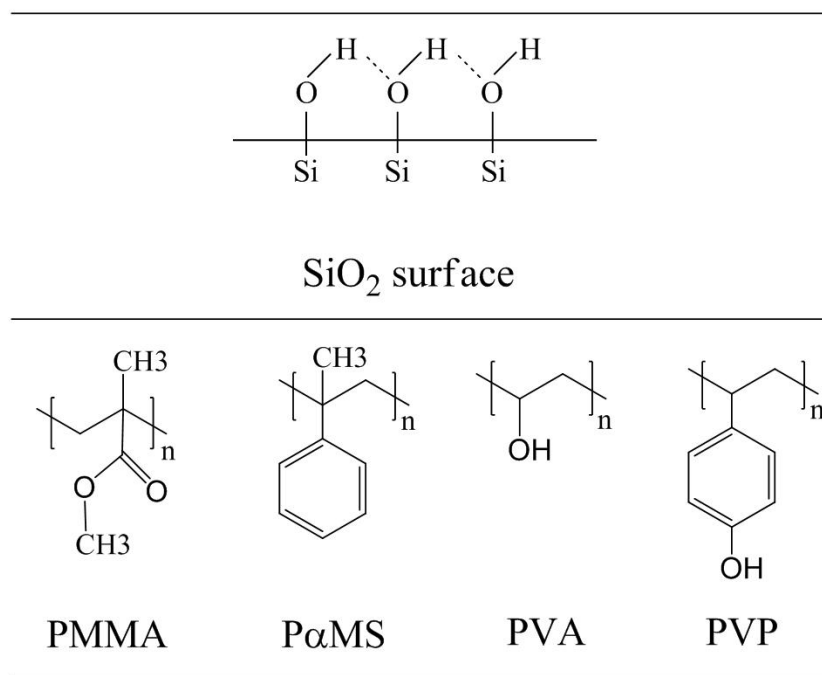
Figure 3. 2 The untreated surface of SiO_2 substrate and the chemical formulation of poly(methyl methacrylate) [PMMA], poly-α-methylstyrene [PαMS], poly(vinyl alcohol) [PVA], and poly(4-vinylphenol) [PVP].

Polymer solutions were spin-coated upon the SiO_2 surfaces pretreated with UV-ozone for 20 minutes. The polymer dielectric materials include poly(methyl methacrylate) [PMMA], poly-α-methylstyrene [PαMS], poly(4-vinylphenol) [PVP], and poly(vinyl alcohol) [PVA], the chemical formulations of which are shown in Figure 3.2.

PMMA and PαMS were dissolved in toluene and each concentration was 1.0 wt %; PVA was dissolved in deionized water and the concentration was 2.0 wt %; PVP and poly(melamine-*co*-formaldehyde) methylated, working as a cross-linking agent, were solved in propylene glycol monomethyl ether acetate. Furthermore, the concentration of PVP is 3.0 wt % and the ratio of PVP to poly(melamine-*co*-formaldehyde) methylated is 2:1. The PVP films were firstly baked at 120°C for 5 min, and then 200°C for 20 min. The other three kinds of polymer films were thermally annealed at 100 °C for 1 hour. The details of procedures are also showed in Figure 3.3. Furthermore, the thickness of each polymer dielectric film was around 70 nm, which was measured by a Digital Instruments Dimension 3100 atomic force microscope (AFM).
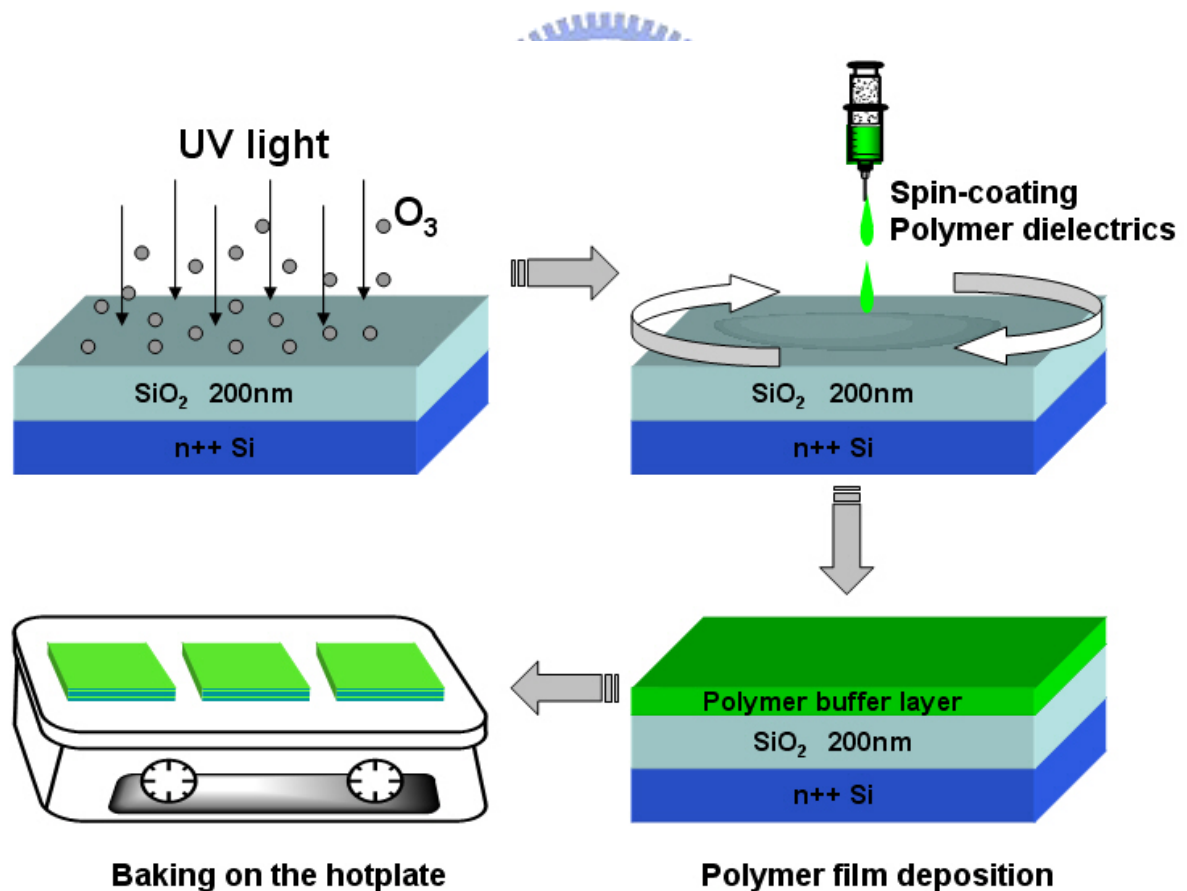
Figure 3. 3   The procedure of polymer thin film deposition.

3.1.4 Growth of Thin Films and Electrodes

Figure 3.4 shows the process of thin-film deposition and electrodes fabrication. 98.0% N,N'-dioctyl-3,4,9,10-perylene tetracarboxylic diimide (PTCDI-C8) purchased from Aldrich without purification was employed as the active layer of n-type OTFTs. The organic semiconductor layers, 50 nm PTCDI-C8, were subsequently deposited upon the dielectric layer at room temperature and under a base pressure of 3×10^{-6} torr. As for deposition rate, it was controlled at 0.5 Å/sec by a quartz oscillator during the thin-film formation. A shutter allowed the stable PTCDI-C8 flux to pass until the total thickness approached 50 nm. A shadow mask was used to define the shape of active layer which has 0.3×0.4 cm^2 area.

Evaporative
PTCDI-C8 flow

mask

PTCDI-C8
Polymer buffer layer
SiO₂ 200nm
n++ Si

50 nm PTCDI-C8 was subsequently deposited on the polymer insulators at a base pressure of 3×10^{-6} torr and at room temperature, and depositing rate was controlled at 0.5 Å/sec.

Evaporative Au flow

mask

S D
PTCDI-C8
Polymer buffer layer
SiO₂ 200nm
n++ Si

40 nm Au, serving as top-contact electrodes, was deposited at 2 Å/sec rate through a shadow mask under 3×10^{-6} torr.

Figure 3. 4 The fabricating process of semiconducting active layer and electrodes.

To complete the devices, gold (99.9%) were vacuum deposited through a shadow mask to serve as source and drain electrodes. In addition, 40 nm Au, serving as top-contact electrodes, was deposited at 2 Å/sec rate through a shadow mask under 3×10^{-6} torr. The channel length (L) and width (W) were respectively 90 μm and 2000 μm. The completed procedure of device fabrication is shown in Figure 3.5.
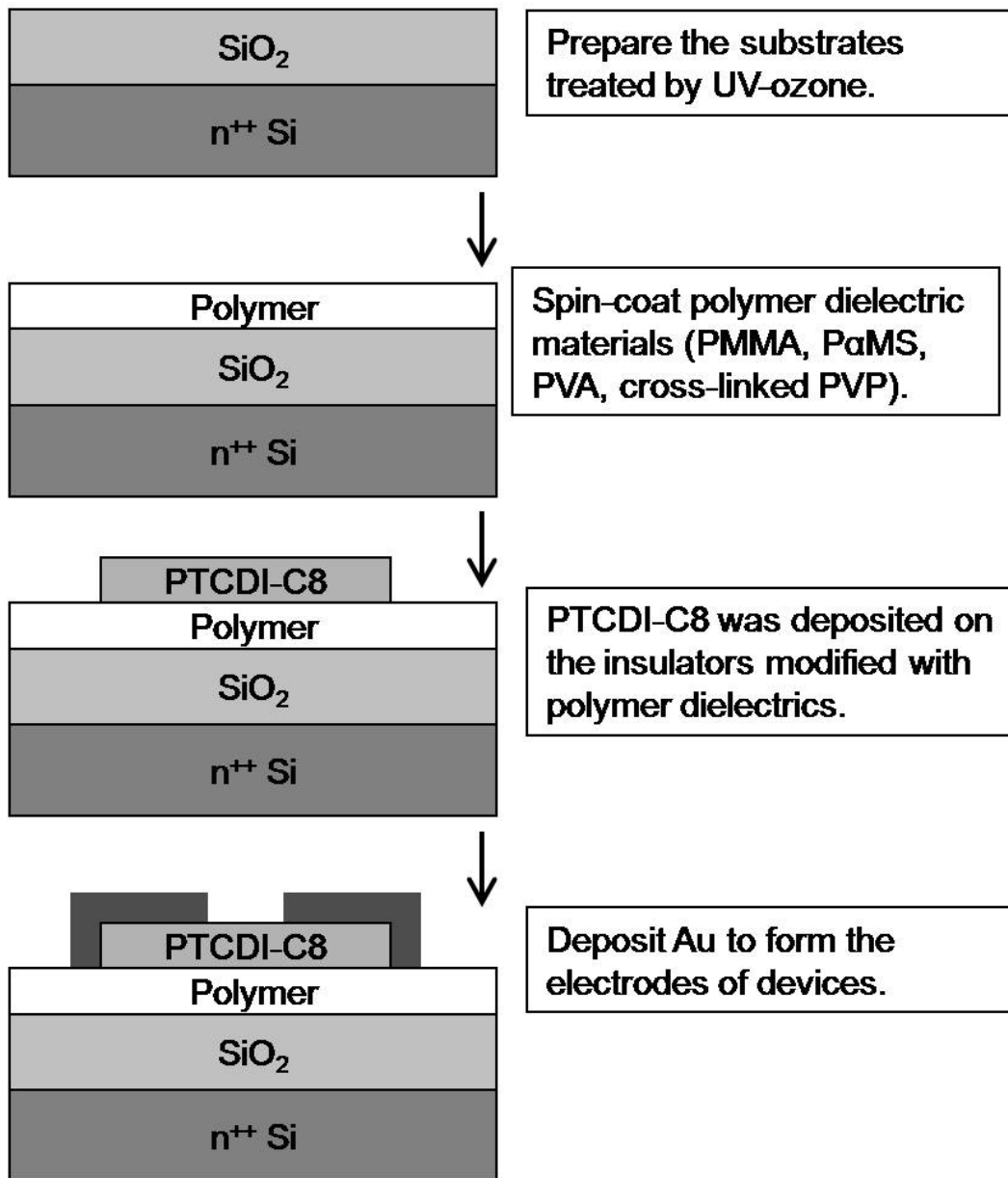
Figure 3. 5   The flow chart of the procedure of device configuration.

3.2 Electrical Measurement of Devices

The electrical properties of the devices were measured by Keithley 4200 IV analyzer in a light-isolated probe station at room temperature. For the devices based on PTCDI-C8, a positive bias of gate voltage was applied to accumulate electrons in the n-channel active layer. In the I_D-V_D measurement, the drain-to-source bias was swept from 0 to 60 Volts and the gate voltage step was 15 Volts from $V_G = 0$ V to $V_G = 60$ V. Besides, in the I_D-V_D measurement, the gate bias was swept from -20 to 60 Volts and the drain-to-source voltage step was 15 Volts from $V_G = 0$ V to $V_G = 60$ V.

The capacitances of insulating layer modified with various polymer dielectric materials were measured by HP4284A using metal-insulator-metal (MIM) structure.

3.3 Surface Morphology Measurement

In our work, we used Digital Instruments Dimension 3100 atomic force microscope (AFM) to obtain the surface morphology of the organic semiconducting layers. By the interaction of the van der Waals force between the tip of the cantilever and the surface topology of the sample, the cantilever vibrates at various frequencies depending on the magnitude of the interaction. Detecting a laser beam reflected by the cantilever can sense the tiny vibration of the cantilever. The computer record these detected signals and construct the surface morphology of samples. Figure 3.6 illustrates the configuration of AFM. From the surface morphology, we have clues to recognize the relation between the transfer characteristics and the graining formation of the organic semiconductor.
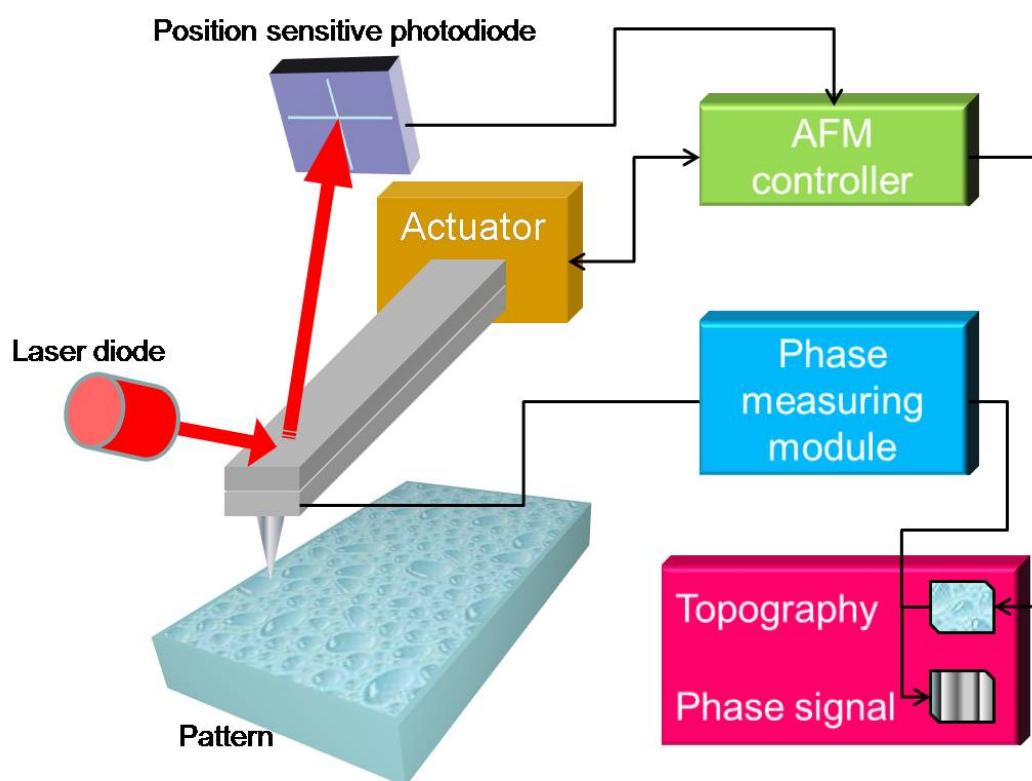
Figure 3. 6 A schematic model of atomic force microscope.
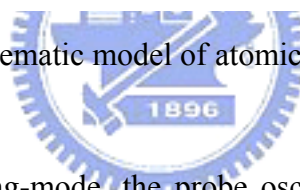
During the scanning of tapping-mode, the probe oscillates up and down regularly. It prevents the probe from damaging the surface of the organic samples and obtains extra topographic information about the samples. The computer records the feedback amplitude and the phase signals of the cantilever. From the amplitude signals we can obtain the morphology information. The phase signals revealed the different materials or arranged formation of the sample.

3.4 Contact Angle Measurement

The contact angle, formed between the liquid/solid interface and the liquid/vapor interface, is defined by the edge of a liquid droplet on the surface of flat sample, which is illustrated in Figure 3.7. Indices s and l stand respectively for "solid" and "liquid"; the

symbols σ_s and σ_l describe the surface tension components of the two phases; symbol γ_{sl} represents the interfacial tension between the two phases, and θ stands for the contact angle corresponding to the angle between vectors σ_l and γ_{sl}.
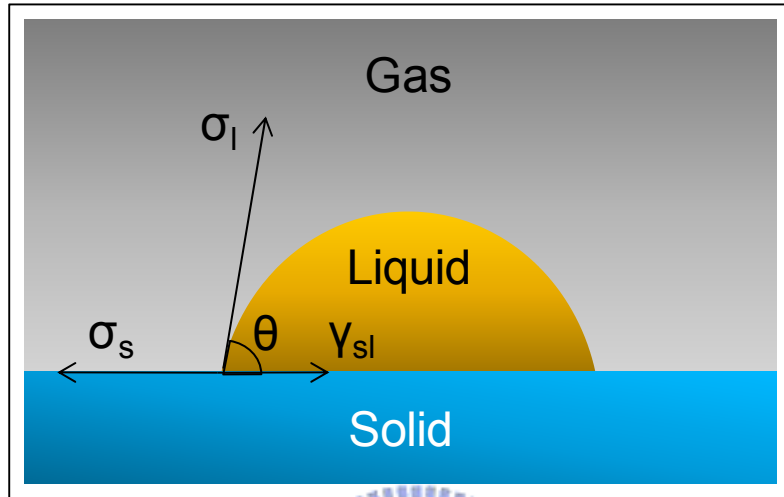
Figure 3. 7   The contact angle formation of liquid on solid surface.

The contact angle is specific for any given system and is determined by the interactions across the three interfaces. The concept of static measurement mode is illustrated with a small liquid droplet resting on a flat horizontal solid surface. This method is used to estimate wetting properties of a localized region on a solid surface.

We dropped respectively diiodo-methane, water and ethylen glycol liquids on the SiO_2 surfaces with various modification to measure the contact angle in each case. Furthermore, use Young's equation[30] to calculate the surface energy of different modified insulators. The contact angle measurement and surface energy calculation were finished by Kruss Universal Surface Tester, GH100.

$$\text{Young's equation} : \sigma_s = Y_{sl} + \sigma_l \times \cos\theta$$

3.5 Instruments

- Vacuum Oven: Yield Engineering Systems, YES-5.

- Spin Coater: Chemat Technology, KW-4A.

- Thermal Coater: ULVAC, CRTM-6000.

- Semiconductor Parameter Analyzer: Keithley 4200.

- Atomic Force Microscope: DI3100.

- X-ray Diffraction: PANalytical X'Pert Pro (MRD).

- Contact Angle: Kruss Universal Surface Tester, GH100.

- Capacitance Measurement: HP4284A.

Chapter 4
Results and Discussion

4.1 Standard Parameters of Each Insulator

From section 2.4, the capacitance of insulator was the first parameter we had to extract before fabricating organic field-effect transistors. Because we had different conditions for the insulators with surface modification, the effective capacitances for different polymer dielectric materials on SiO_2 insulators were not the same. Table 4.1 lists the parameters of the fabricated polymer insulators under different conditions.

Table 4. 1   The conditions and parameters of polymer insulating layers.

Polymer Dielectrics	PMMA	PαMS	PVA	PVP
Solvent	Toluene	Toluene	H_2O	PGMEA
Concentration	1wt%	1wt%	2wt%	3wt%
Deposition Condition	Spin-coating 500rpm/10s → 2000rpm/40s			
Baking Temp	100℃/60min			120℃/5min 200℃/20min
Thickness	~70 nm			

The dielectric polymer solution was spun upon 200 nm SiO_2 and then the capacitances of polymer insulators and SiO_2 were must counted in the totally effective capacitance. The resulting capacitance of bilayer was regarded as series-connected capacitances of 70 nm polymer insulator and 200 nm SiO_2 layer. Table 4.2 illustrates the totally effective capacitance of each case.

Table 4. 2 The capacitance of the bilayer insulators with dielectric polymers and SiO_2.

	PMMA/SiO_2	PαMS/SiO_2	PVA/SiO_2	PVP/SiO_2	SiO_2
Thickness (nm)	70/200	70/200	70/200	70/200	200
C_i (nF/cm^2)	10.0	10.3	12.5	9.4	14.2

4.2 Electrical Characteristics

In our work, substantially improved air-stability of n-channel OTFTs based on N,N'-dioctyl-3,4,9,10-perylene tetracarboxylic diimide (PTCDI-C8), which was not considered as an air-stable n-channel organic semiconductor,[31] is obtained by modifying the dielectric surface with insulating polymer. In addition, we wanted to investigate the phenomenon of PTCDI-C8 OTFTs with various surface modifications on SiO_2 layer due to the sensitivity of n-type organic transistors on H_2O and O_2 in ambient atmosphere. The following are the discussions of electrical transfer characteristics on various devices operated in different environments.
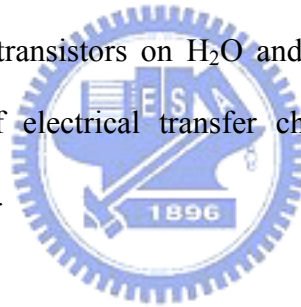
4.2.1 Electrical Measurement under Inert Condition

We firstly measured these devices with various insulating polymer modifications in a N_2-filled glove box such serving as an inert environment in which there were lower concentrations of O_2 ($\leq$1ppm) and H_2O ($\leq$1ppm). Figure 4.1 illustrates the I_d-V_d electrical performances in each device which had distinct dielectric surface. From Figure 4.1 (a) to (e), they represent the devices with dielectric surface of SiO_2, PMMA, PαMS, PVA, and cross-linked PVP, respectively. The devices with modifications of PVA and cross-linked PVP have lower drain current in the saturation regime. Although silanols (SiOH) present on the SiO_2 surface, the device still exhibited well electrical transfer behaviors in inert environment. The best performances were obtained in PMMA and PαMS cases, and the result was also shown in the I_d-V_g characteristics (Figure 4.2).
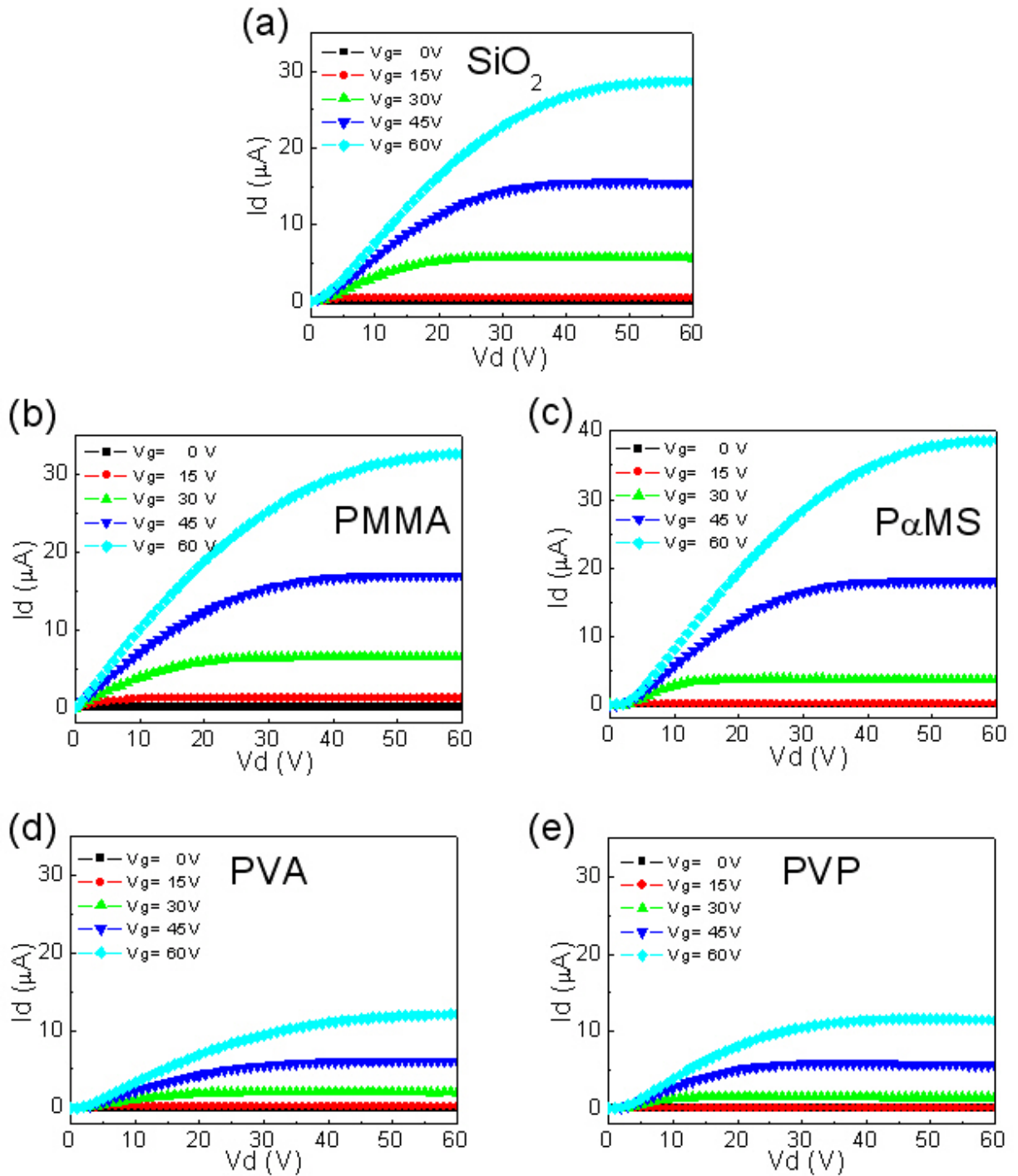
Figure 4. 1 The I_d-V_d electrical transfer performances of the transistors with distinct dielectric surfaces in a N_2-filled glove box, and they represent the devices modified with (a) SiO_2, (b) PMMA, (c) PαMS, (d) PVA, and (e) cross-linked PVP, respectively.
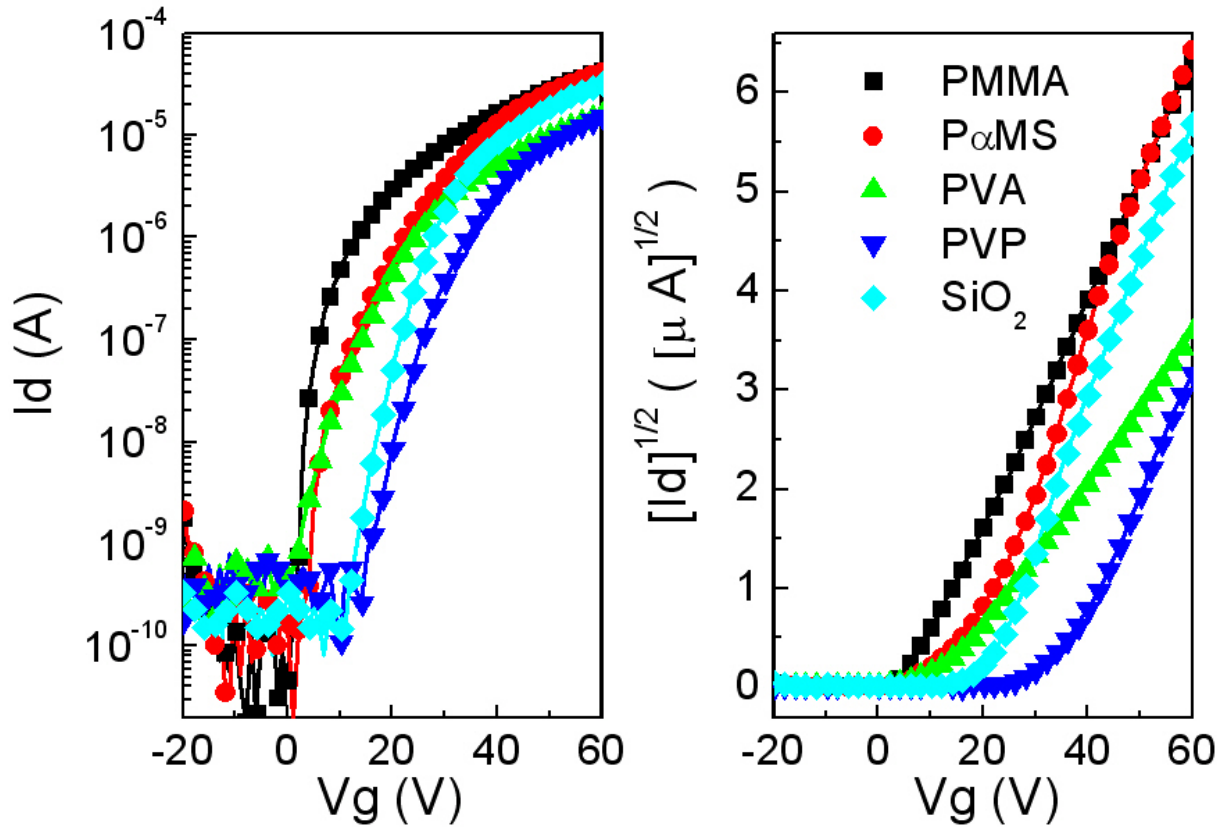
Figure 4. 2 The I_d-V_g electrical transfer performances of the transistors with distinct dielectric surfaces in a N_2-filled glove box.

The data shown in Figure 4.2 were measured at $V_d = 60$ V and V_g bias was swept from 0 to 60 V. Furthermore, the electron mobilities were calculated from the slopes of square root of drain current versus gate voltage in the saturation region, and the other important extracted parameters were also shown in Table 4.3. The devices modified with PMMA and PαMS had higher on-off current ratios (4.8×10^5 and 2.4×10^5, respectively), and then showed lower threshold voltages (7.01 V and 18.43 V, respectively). The subthreshold swing (S.S.) of PMMA and PαMS devices were 1.20 and 1.56 V/decade, respectively. After all, their performances were better than the other devices with SiO_2, PVA, and cross-liked PVP dielectric surfaces. The transfer behavior (I_d-V_g curve) of PMMA device was the best one, as illustrated in Figure 4.2, but the mobility of PMMA device (0.141 cm^2/Vs) was similar to that of SiO_2 (0.127 cm^2/Vs) and cross-liked PVP (0.161 cm^2/Vs) devices.

Moreover, the highest electronic mobility obtained from the device with PαMS dielectric surface was 0.327 cm^2/Vs.

Table 4. 3 The comparison of transfer characteristics of PTCDI-C8 OTFTs measured under inert condition (N$_2$-filled glove box).

Dielectrics	Mobility (cm^2/ Vs)	On/off	V_{Th} (V)	S.S. (V/decade)
PαMS	0.327	2.4×10^5	18.43	1.56
PMMA	0.141	4.8×10^5	7.01	1.20
PVP	0.161	4.0×10^4	27.41	4.11
SiO$_2$	0.127	1.7×10^5	19.13	3.03
PVA	0.056	4.3×10^4	12.40	4.34

4.2.2 Electrical Measurement in Atmosphere

We further measured these devices in ambient environment in which the relative humidity was around 50%-55%. Figure 4.3 illustrates the I_d-V_d electrical transfer performances in each case which had distinct dielectric surface. From Figure 4.3 (a) to (e), they respectively represent the output characteristic of the devices with dielectric surface of SiO$_2$, PMMA, PαMS, PVA, and cross-linked PVP.

The devices with modifications of PVA and cross-linked PVP had much lower drain current. In addition, the drain currents of cross-linked PVP device decreased unsteadily when increasing the drain-to-source bias in saturation mode, and so did the device with bare SiO$_2$ insulator. There was dramatic decay of transfer performance present on SiO$_2$, PVA, and cross-linked PVP devices while storing them in ambient environment. The best performances were also obtained in PMMA and PαMS cases, and they had a relatively air-stable transfer characteristic. Moreover, the transfer characteristics of drain current versus gate voltage are also shown in Figure 4.4.
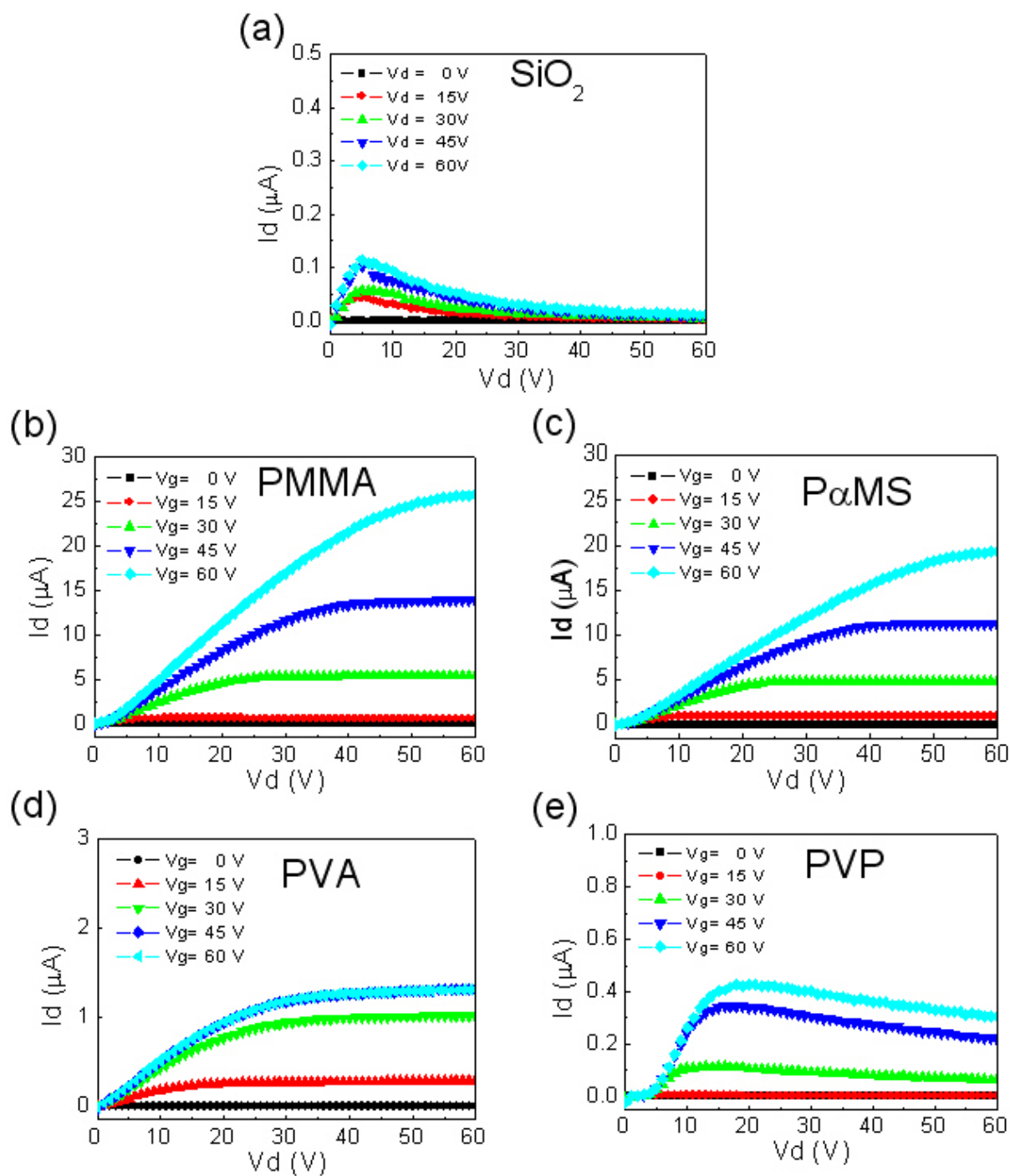
Figure 4. 3 The I_d-V_d electrical transfer performances in each case which had distinct dielectric surface in ambient environment, and they respectively represent the devices modified with (a) SiO_2, (b) PMMA, (c) PαMS, (d) PVA, and (e) cross-linked PVP.

From Figure 4.3 and Figure 4.4, the performances of the device without modification on SiO_2 insulator surface showed an unstable transfer characteristic and decayed rapidly in ambient environment. Although the devices with modifications of PVA and cross-linked PVP still worked in ambient air but the saturated drain currents were such relatively smaller. Especially, Table 4.4 illustrated the transfer performances of these devices in ambient atmosphere. The mobility and on-off ratios in the cases of PVA and PVP decreased obviously from inert to ambient condition. In PVA case, the threshold voltage shifted from 12.4 V to 20.22 V and the mobility decreased from 0.056 cm^2/Vs to 0.015 cm^2/Vs. Furthermore, in PVP case, the threshold voltage also exhibited a positive shift from 27.41 V to 42.20 V and the mobility even had an apparent decay from 0.161 cm^2/Vs to 0.022 cm^2/Vs.
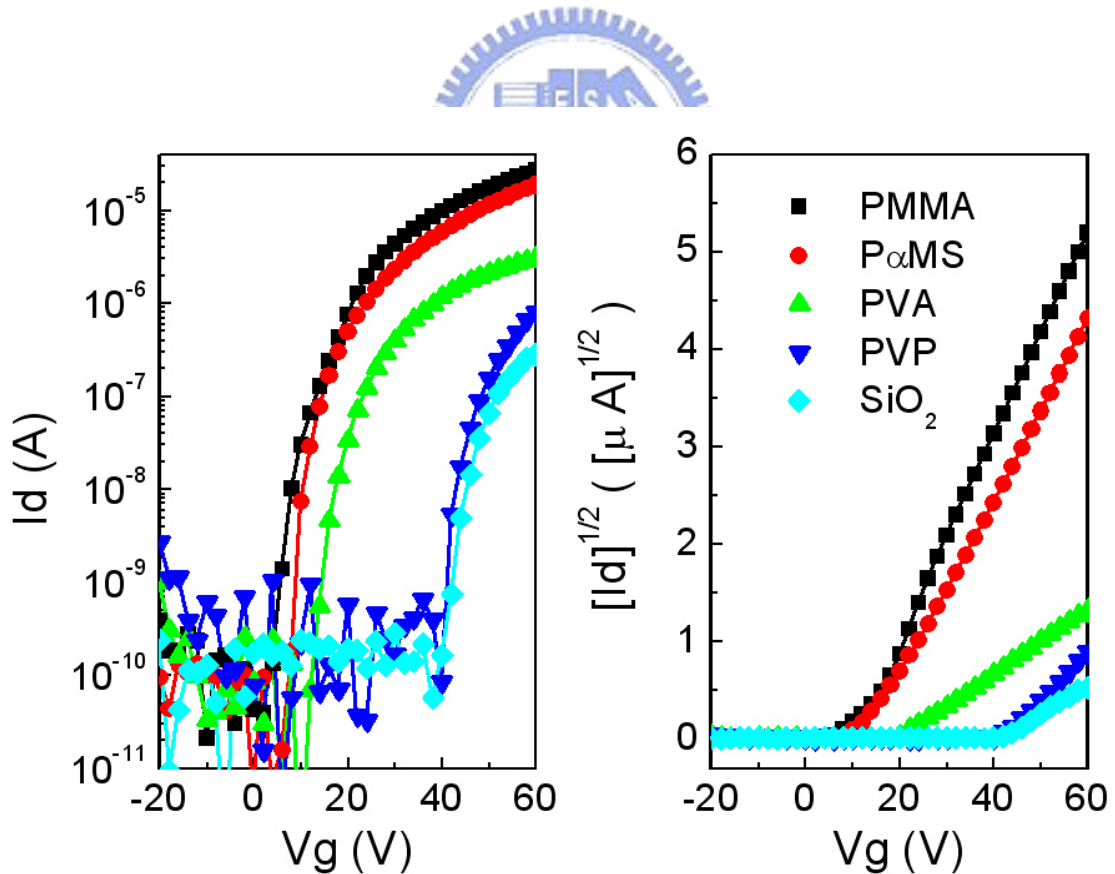
Figure 4. 4 The I_d-V_g electrical transfer performances in each case which had distinct dielectric surface in ambient atmosphere.

In the view of air-stability of n-channel OTFTs, PMMA modification upon SiO_2 surface seemed to be a better choice. The transfer behavior stayed stably even in the ambient atmosphere involved with O_2 and H_2O, and the field-effect electronic mobility still kept at 0.11 cm^2/Vs.

Table 4. 4 The comparison of transfer characteristics of PTCDI-C8 OTFTs measured in ambient environment.

Dielectrics	Mobility (cm^2/ Vs)	On/off	V_{Th} (V)	S.S. (V/decade)
PMMA	**0.11**	**3.3×10^5**	**10.72**	**1.96**
PαMS	0.09	3.0×10^5	15.01	1.69
PVP	0.022	4.4×10^3	42.20	1.60
PVA	0.015	3.1×10^4	20.22	2.22
SiO_2	0.006	1.0×10^3	43.25	3.06

4.2.3 Long-time Test

In order to identify the air-stability of PTCDI-C8 OTFTs modified with hydroxyl-free polymer dielectric surfaces, these devices were measured through 60 days both in ambient atmosphere and N_2-filled glove box. From Figure 4.5 (a), stable mobilities could be obtained in each case in 60 days in an inert environment, even though a little decay existed in the last 30 days. In addition, the on-off current ratios also performed stably even after 60 days, such as shown in Figure 4.5 (b).

For the device with PMMA polymer dielectric modification, the mobility was 0.141 cm^2/Vs in the first day and became 0.105 cm^2/Vs after 60 days in glove box. The on-off ratio was still larger than 10^5 until the 60th day and decayed inconspicuously from 4.8×10^5 to 3.2×10^5. However, the mobility in the PαMS device exhibited the value of 0.171 cm^2/Vs which was close to the half of initial mobility of 0.327 cm^2/Vs and decayed a little faster than that of the PMMA device. Even though the on-off ratio of the PαMS device (2.4×10^5)

is smaller than that of the PMMA device (4.8×10^5), the on-off ratio is more stable for the PαMS device. The other cases had similar results as shown in Table 4.5 and Table 4.6 which list the comparison of the transfer characteristics in different condition.
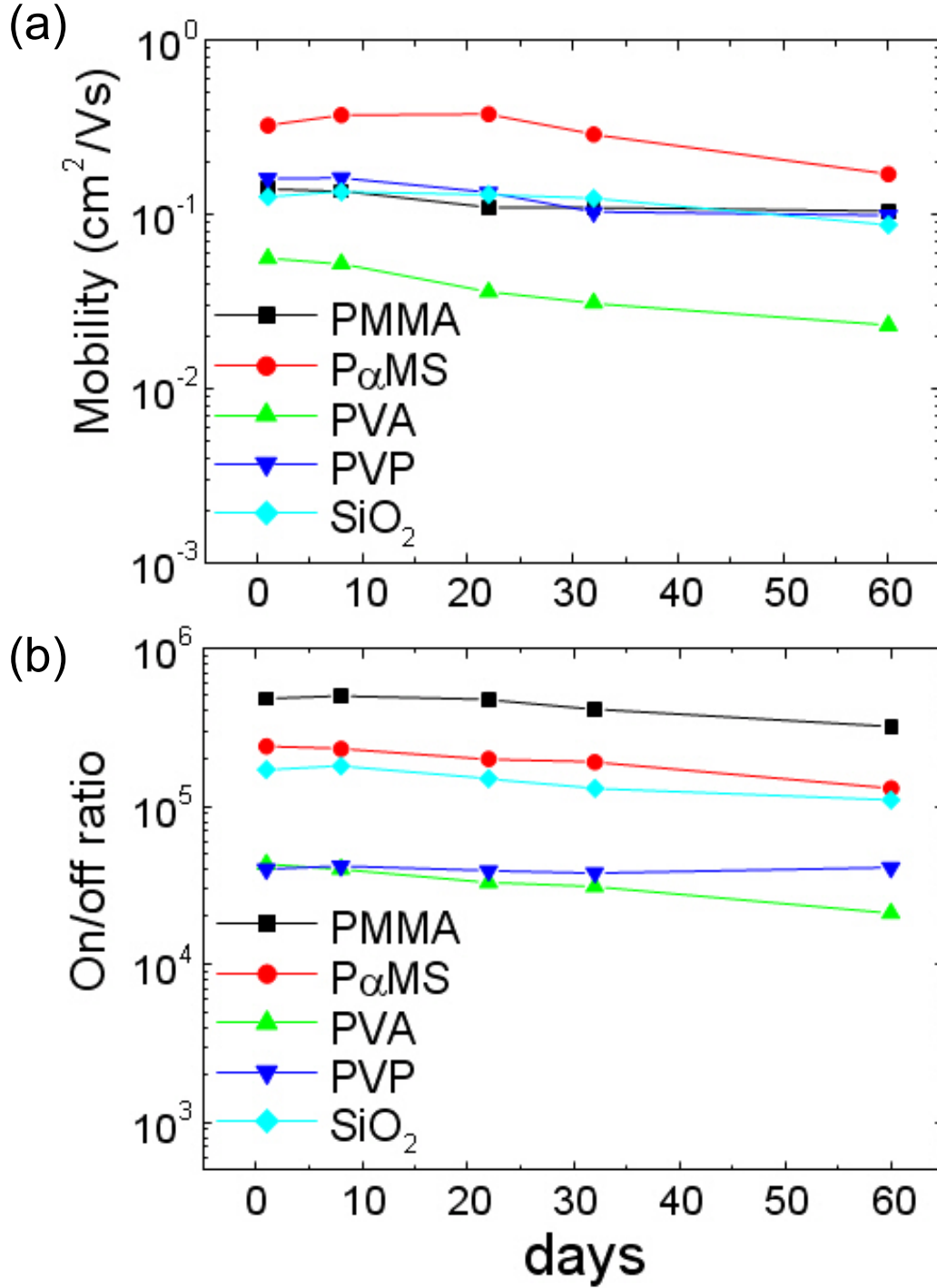
Figure 4. 5 Long-time testing for transfer characteristic measurement in inert environment. (a) the mobility and (b) the on-off ratio in the duration of 60 days.

Figure 4.6 illustrated the performing stability of mobilities and on-off ratios by operating these devices in ambient environment. The relative humidity during the period of measurement was controlled around 50%~55%. The devices modified with PMMA and PαMS exhibited better air-stability than the device with bare SiO_2 and PVP and PVA modified dielectrics. Take the device containing PMMA as the modified layer for example, the electron mobility and the on-off ratio both stayed almost unchanged after ~15 days. The mobility dropped to 0.05 cm^2/Vs at the 29th day, and eventually to 0.03 cm^2/Vs after 60 days. Further, the PαMS device also exhibited similar air-stability compared with that of the PMMA device. Ultimately, the mobility expressed a reduction to 0.04 cm^2/Vs after 60 days in the PαMS device.

While the dielectric buffer layer was either PVP or PVA, both the device mobilities and on-off ratios dropped rapidly. In addition, the mobilities dropped to 10^{-4}~10^{-5} cm^2/Vs and the on-off ratios decreased to less than the order of 10^2 in PVP and PVA devices after 15 days in ambient atmosphere. The PVA and PVP devices exhibited poorer n-channel air-stability than that of PMMA and PαMS devices, and even no apparent field effect could be observed after 20 days.

Moreover, the field-effect behavior of bare SiO_2 device existed less than one week, and therefore the transfer performances were not shown in the figure of long-time test in atmosphere. After all, the PTCDI-C8 transistors with hydroxyl-free dielectric modification on SiO_2 insulator surface had a better air-stable field-effect characteristic, such as PMMA and PαMS.
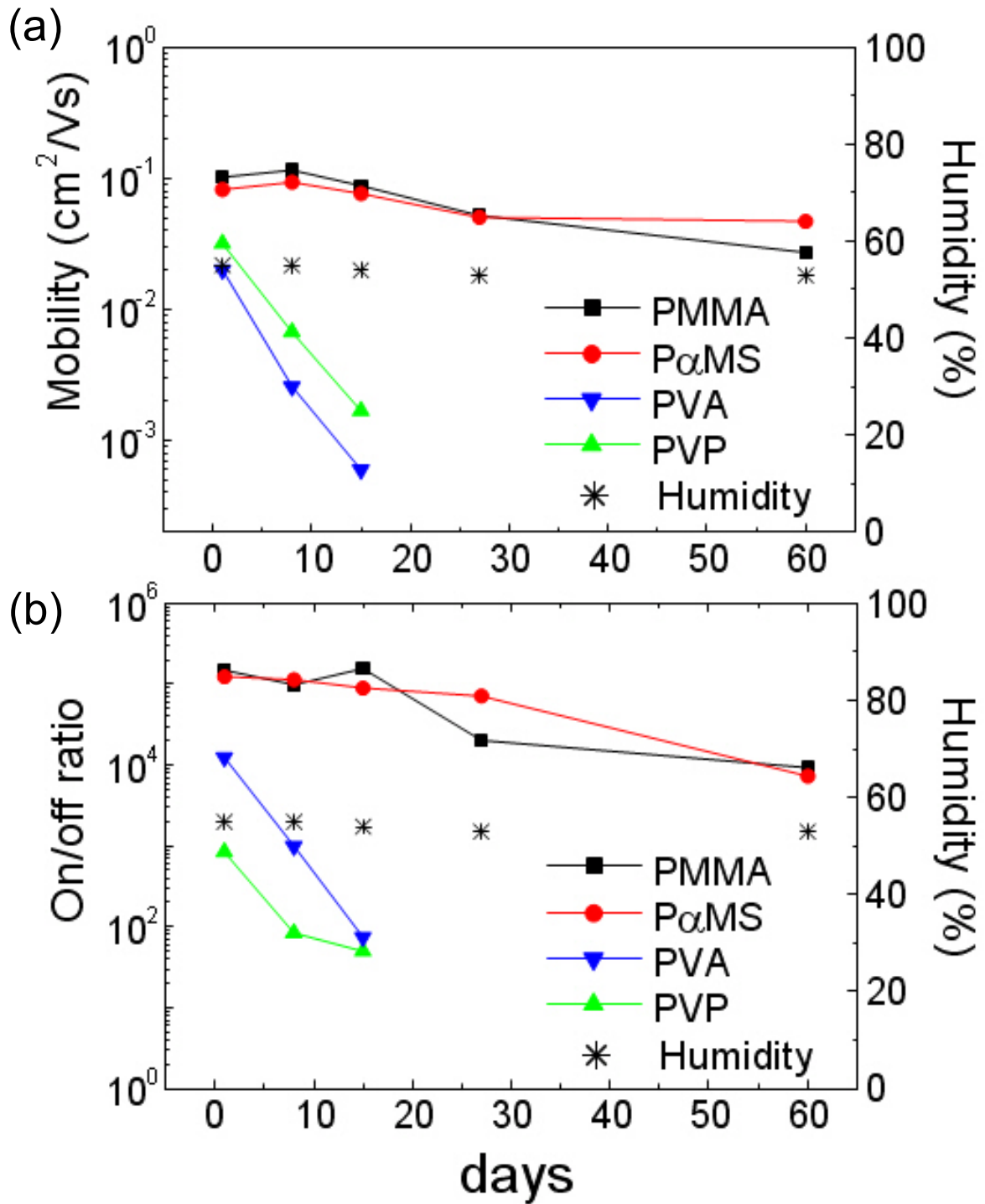
Figure 4. 6 Long-time testing for transfer characteristic measurement in ambient atmosphere. (a) the mobility and (b) the on-off ratio in the duration of 60 days.

Table 4.5 compared the mobilities measured in ambient and inert conditions for the PTCDI-C8 devices with different dielectrics surfaces. Further, the stability of on-off current

ratios, obtained in N_2-filled glove box and ambient atmosphere, expressed different tendencies as shown in Table 4.6. Eventually, the relative recessions of the PMMA and PαMS devices from inert to ambient condition presented better performances.

On the other hand, for the devices with hydroxyl groups on the dielectric surface (SiOH, PVA or PVP), there is significant decay of transfer characteristics from inert environment to ambient atmosphere present here.

Table 4. 5 The comparison of mobilities between ambient and inert conditions for PTCDI-C8 devices with different dielectrics surfaces.

Dielectric	Mobility (cm^2/Vs)				
	N_2-filled glove box		Atmosphere		
	1st day	60th day	1st day	15th day	60th day
PMMA	0.141	0.105	0.110	0.088	0.030
PαMS	0.327	0.171	0.090	0.076	0.047
PVP	0.161	0.099	0.022	$5.9×10^{-4}$	---
PVA	0.056	0.023	0.015	$8.5×10^{-5}$	---
SiO_2	0.127	0.087	0.006	---	---

Table 4. 6 The comparison of on-off ratios between ambient and inert conditions for PTCDI-C8 devices with different dielectrics surfaces.

Dielectric	On-off ratio				
	N_2-filled glove box		Atmosphere		
	1st day	60th day	1st day	15th day	60th day
PMMA	$4.8×10^5$	$3.2×10^5$	$3.3×10^5$	$1.5×10^5$	$9.3×10^4$
PαMS	$2.4×10^5$	$1.3×10^5$	$3.0×10^5$	$9.0×10^4$	$7.2×10^3$
PVP	$4.0×10^4$	$4.1×10^4$	$4.4×10^3$	$6×10^1$	---
PVA	$4.3×10^4$	$2.1×10^4$	$3.1×10^4$	$8×10^1$	---
SiO_2	$1.7×10^5$	$1.1×10^5$	$1.0×10^3$	---	---

In the following sections, we would use different aspects to confirm the results obtained by electrical measurement and attempt to explain the mechanism on the PTCDI-C8 OTFTs with different dielectric surface modifications.

4.3 X-ray Diffraction Analysis

The crystallinity of the PTCDI-C8 thin films was studied by Gonio-scan X-ray diffraction (XRD) using PANalytical X'Pert Pro (MRD) system with a Cu Kα (λ= 1.54 Å) source. Figure 4.7 illustrates the XRD spectra of 20 nm PTCDI-C8 on various dielectrics. In 2004, Chesterfield *et al.* expressed the OTFTs based on PTCDI derivatives and showed the similar PTCDI-C8 diffraction patterns as our results.[32] The spectra of PTCDI-C8 upon different dielectric surfaces exhibit no thin film phase and there is a sharp primary peak (2θ = 4.28°) with a *d* spacing of 20.06 Å.
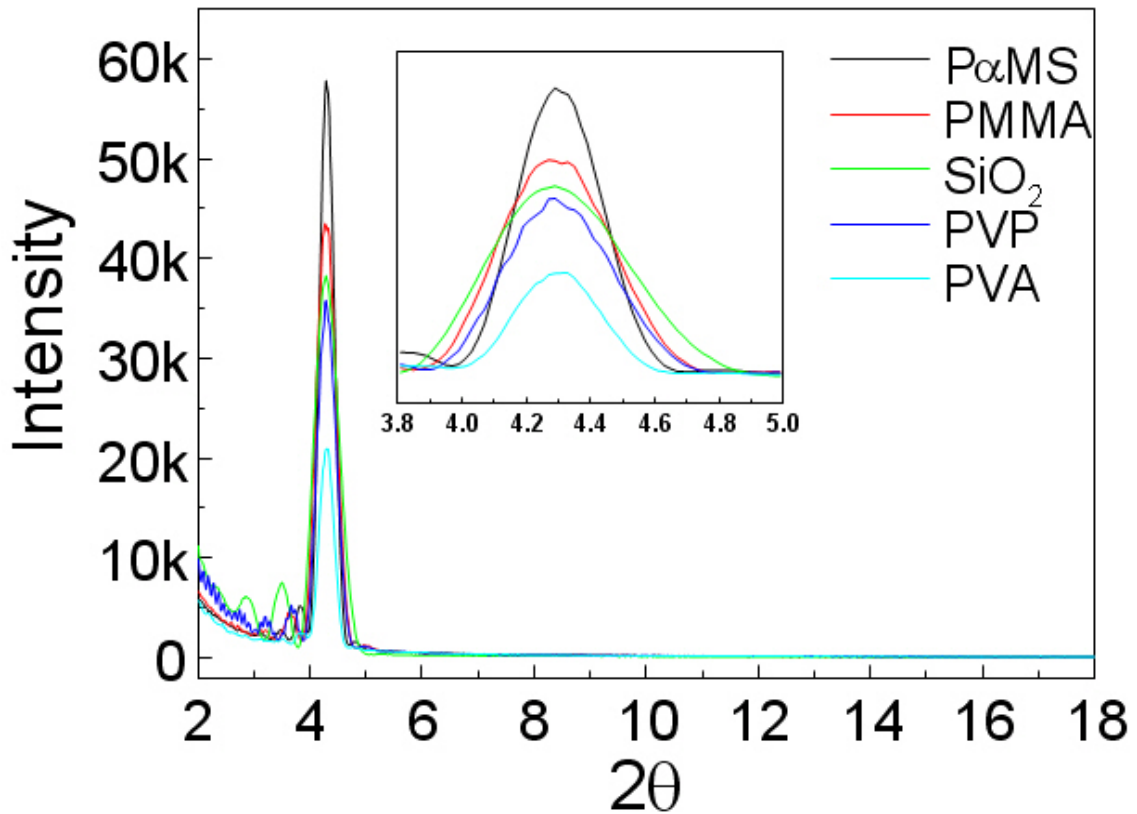
Figure 4. 7 X-ray spectra of 20 nm PTCDI-C8 deposited at a fixed flux rate of 0.5 Å/sec on different dielectric surface, PαMS, PMMA, PVP, PVA, and SiO₂, at room temperature. Insert is the XRD spectra near the maximal diffracted angle of 4.28°.

Table 4.7 exhibits the relationship between the crystalline order and the field-effect performances. While better crystallinity was obtained, the higher electronic mobility was also obtained in inert environment. Take the performances of the devices concerning PMMA and PVP into consideration. Even though the normalized primary peak of PTCDI-C8 on PVP is smaller than that of PMMA which has a little wider full-width at half-maximum of diffracted intensity (FWHM = 0.205°), the mobility of the PVP device exhibited somewhat higher than that of PMMA but the variation was not notable. Take notice of the other aspects, the performances on on-off ratio, threshold voltage, and subthreshold swing of PMMA device are much better than those of the PVP device. After all, the overall transfer behaviors in PMMA device had better performances than those of the PVP device (Figure 4.2). Thus, the crystalline quality of PTCDI-C8 thin film could determine not only the mobilities but also the other transfer representation in inert condition. In terms of the confrontation between the crystallinity and electrical performance, the PTCDI-C8 OTFTs with PMMA and PαMS modification on insulator had better crystalline growth to identify why the relative better transfer characteristics could be performed.

Table 4. 7 The comparison between the results of XRD spectra and field-effect transfer characteristics.

Dielectric	Mobility (cm^2/ Vs)	On/off	V_{Th} (V)	S.S. (V/decade)	Normalized intensity at primary peak	FWHM (°)
PαMS	0.327	2.4×10^5	18.43	1.56	1	0.16
PMMA	0.141	4.8×10^5	7.01	1.20	0.75	0.205
PVP	0.161	4.0×10^4	27.41	4.11	0.62	0.20
SiO$_2$	0.127	1.7×105	19.13	3.03	0.66	0.26
PVA	0.056	4.3×10^4	12.40	4.34	0.36	0.16

4.4 Atomic Force Microscope Analysis
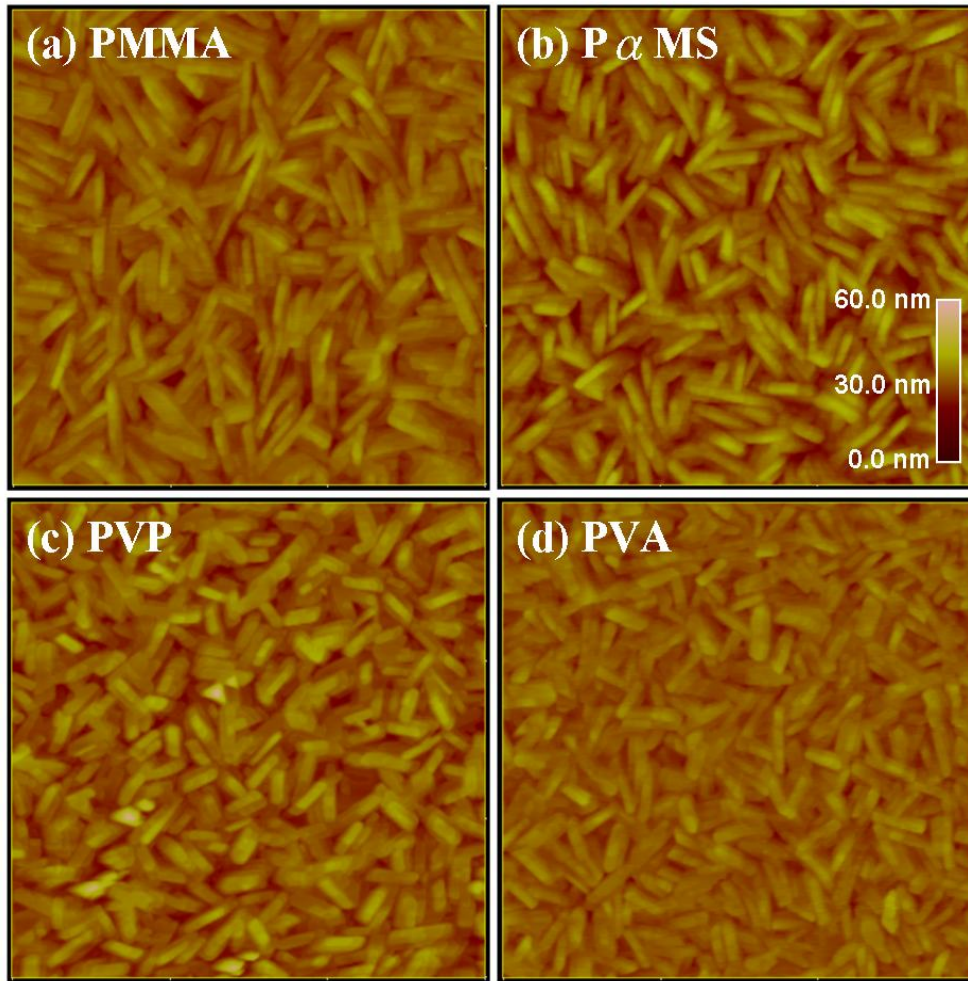
Figure 4. 8   (a)-(d) the 3×3 μm² morphology images of the 50 nm-thick PTCDI-C8 films deposited on PMMA, PαMS, PVP, and PVA, respectively. Inset in (b) is the color scale for all cases.

The morphology of the 50 nm PTCDI-C8 thin films deposited on various polymer dielectric layers was indicated in Figure 4.8. All the surfaces showed typical rod-like grains similar to the grains of PTCDI-C5 films presented in M. Petit *et al*. s' study.[33] Although the grain size of PTCDI-C8 on PVP was slightly different from those of the other three cases, very little difference were observed between the PTCDI-C8 films on PMMA, PαMS and PVA surfaces. As a result, no apparent correlation between the morphology and the ambient device performance was observed.

PTCDI-C8 thin films seem to provide better field-effect transfer characteristics on appropriate polymer surface, such as PMMA and PαMS. Because of the first few monolayers working as an active channel for the transistor, the orientation and morphology of the PTCDI-C8 molecules at the early stages are more important for OTFTs. The AFM images of 7 nm PTCDI-C8 thin films deposited on various modified dielectric surfaces are presented in Figure 4.9 (a)-(e).

The grain size of PTCDI-C8 on PVA was smaller than that of the other cases. Further, the other PTCDI-C8 films, including the one on bare SiO_2 [Figure 4.9 (a)], had similar morphology. The result is actually consistent with the crystallinity of PTCDI-C8 films and device performances measured in a N_2-filled glove box (Table 4.7), where the PVA device exhibits the lowest mobility. Because the smaller grains result in higher density of grain boundaries, the electron transport is disrupted by the traps between these grains. Further compared with the topography, the XRD spectra indicate clearly that the crystallinity of PTCDI-C8 upon PVA surface maybe has complicated phases on the molecular configuration due to the less ordered crystalline orientation of PTCDI-C8.

By Bragg's law, $2d \sin\theta = n\lambda$, the d spacing was determined as 20.06Å in the previous section. The AFM images of 15 nm PTCDI-C8 films as illustrated in Figure 4.9 (f)-(j) establish these layers corresponding to molecular terraces in the film with a terrace height of 20.06±1 Å (Figure 4.10) except for the PVA case. In Figure 4.9 (j), the rectangular regions marked by dotted line exhibit the somewhat rougher and less ordered grains. On the other hand, the better arrangement of PTCDI-C8 is shown such as the region marked by solid line. Due to the unfit growing interface of PVA for the growth of PTCDI-C8, the crystallinity of PTCDI-C8 upon PVA surface illustrated in Figure 4.7 has a relatively less ordered crystalline orientation.
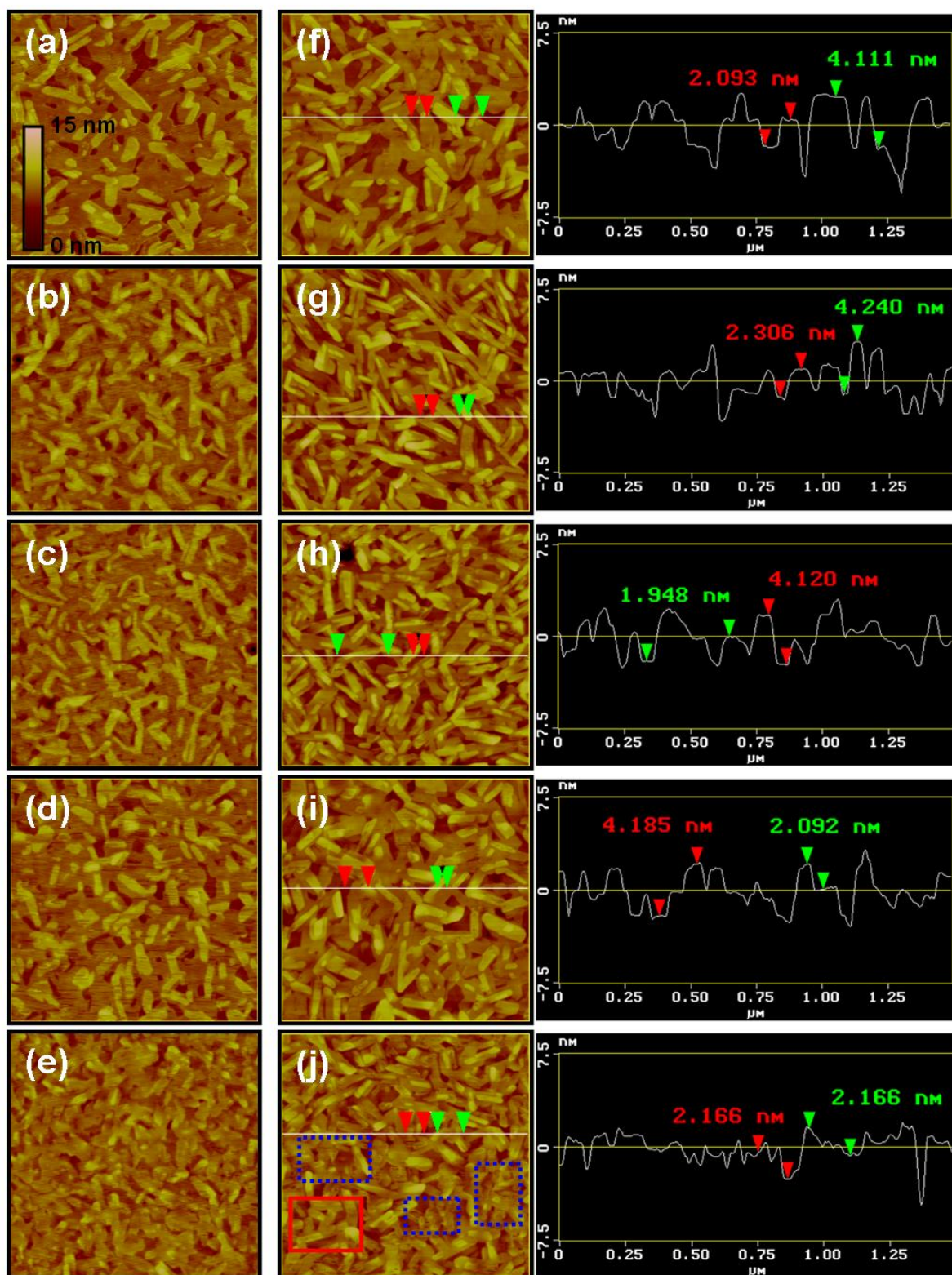
Figure 4. 9 The morphology of the PTCDI-C8 films. (a)-(e) are 1.5×1.5 μm² AFM images of 7 nm-thick PTCDI-C8 thin films deposited on SiO₂, PMMA, PαMS, PVP, and PVA, respectively. (f)-(j) are 15 nm-thick PTCDI-C8 films on SiO₂, PMMA, PαMS, PVP, and PVA, respectively, with corresponding profiles. Inset in figure (a) is the color scale for all cases.
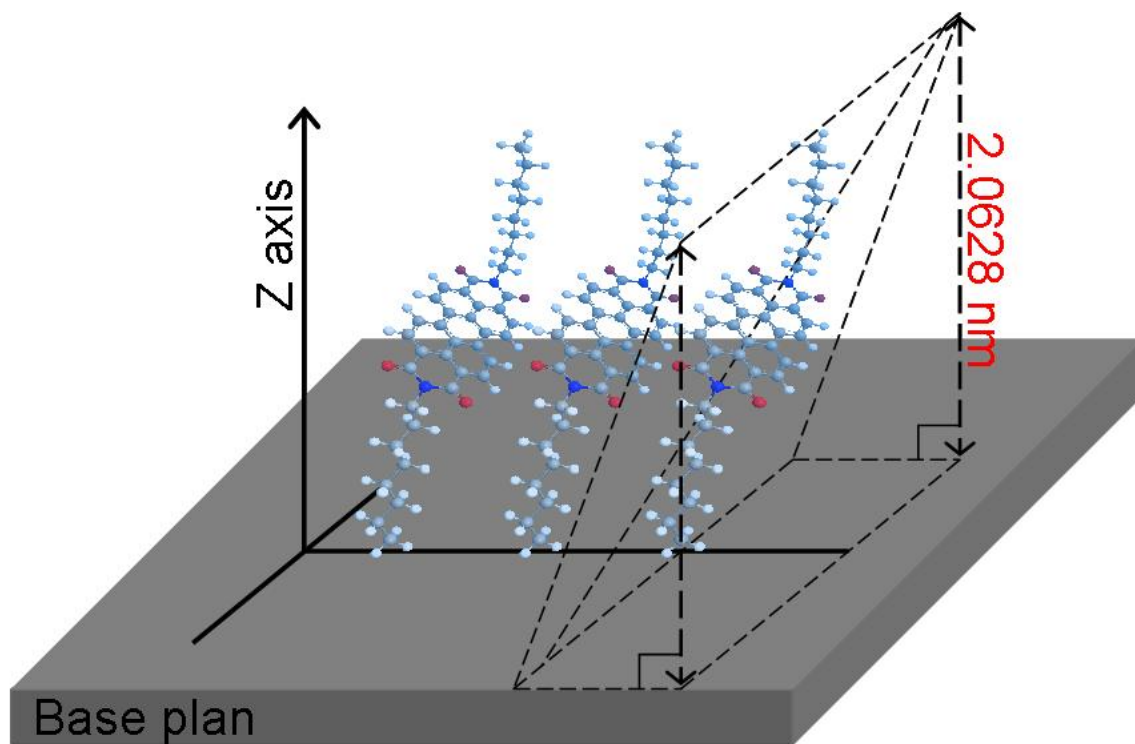
Figure 4. 10   The simulated 3-D picture of PTCDI-C8 molecule alignment for the bulk phase (d spacing, 20.0628 Å).

4.5 Contact Angle and Surface Energy Analysis

From section 4.3 and 4.4, the XRD spectra and AFM images indicate the various dielectric surfaces affecting the growth of PTCDI-C8. The contact angle measurement can show further information about the surface energies on sample surfaces and the hydrophilic property of solid surfaces to assist the recognization of the causes to the air-stability of n-channel OTFTs based on PTCDI-C8. Table 4.8 illustrates the parameters of the testing liquid droplets for measuring the contact angle, The Young's and Wu's approximations was used to calculate the dielectric surface energies.[30,34]

Table 4. 8 The parameters of the testing liquid droplets.

Used Liquids	Surface tension (mN/m)	Disperse part (mN/m)	Polar part (mN/m)
Diiodo-Methane	50.8	50.8	0
Deionized Water	72.8	21.8	51
Ethylen Glycol	48.0	29.0	19

The contact-angle images of the insulators were obtained, and the corresponding contact angles with deionized water droplets were presented in Figure 4.11. In addition, the surface energies and the other contact angles formed by diiodo-methane drops and ethyled glycol droplets for each dielectric surface are illustrated in Table 4.9. The results indicated that the hydrophobic surface affects significantly the growth of PTCDI-C8 (Table 4.10). Compared with the AFM images of 7 nm and 15 nm PTCDI-C8 films, the hydrophilic surface of PVA complicates the orientation of PTCDI-C8 and then causes the crystallinity less regular. On the contrary, the low surface energy of the PαMS may lead to the better crystal orientation on the early stage of PTCDI-C8 crystal formation for effective electron transportation, and results in a higher electron mobility measured in an inert environment.
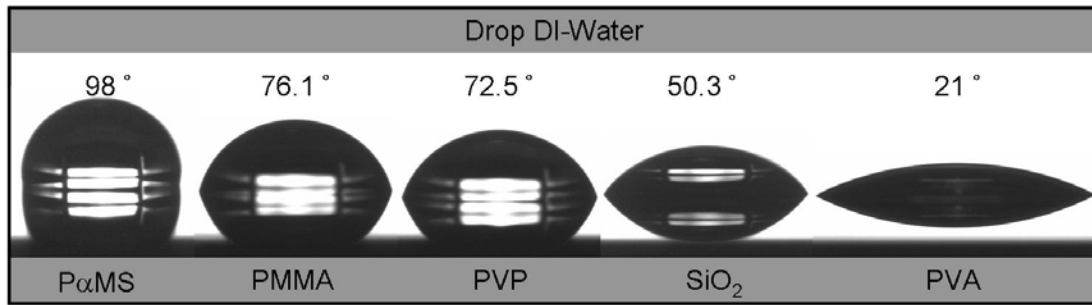
Figure 4. 11 The contact-angle images of deionized water dropping on various substrates which are PαMS, PMMA, PVP, SiO₂, and PVA, respectively.

Table 4. 9 The presentation of contact angle measurement and surface energy.

dielectrics	Contact angle (°)			Surface energy
	diiodo-Methane	H_2O	Ethylen glycol	(mN/m)
PαMS	25.6	98	70.5	24.7
PMMA	35.8	76.1	54.4	37.7
PVP	26.2	72.5	40.3	42.0
SiO₂	40.8	50.3	22.5	45.3
PVA	40.1	21	22.5	55.5

Table 4. 10 The presentation of contact angle measurement compared with the transfer characteristics measured both in inert environment and ambient atmosphere for PTCDI-C8 OTFTs with different polymer dielectrics.

dielectrics	Surface energy (mN/m)	water contact angel (degree)	ambient atmosphere		inert environment	
			mobility (cm^2/Vs)	on/off ratio	mobility (cm^2/Vs)	on/off ratio
SiO₂	45.3	50.3	0.006	1.0×10^3	0.13	1.7×10^5
PαMS	24.7	98.0	0.090	3.0×10^5	0.33	2.4×10^5
PMMA	37.7	76.1	0.11	3.3×10^5	0.14	4.8×10^5
PVP	42.0	72.5	0.022	4.4×10^3	0.17	4.0×10^4
PVA	55.5	21.0	0.015	3.1×10^4	0.056	4.3×10^4

4.6 Discussion of Mechanism

4.6.1 Preface to The Mechanism in Our Work

Figure 4.4 displays the device characteristics of the devices modified with different polymer insulators under ambient atmosphere. Apparently, the devices modified with PMMA and PαMS had higher mobilities and on-off ratios than those of the devices modified with polymers containing hydroxyl groups (PVP and PVA). Further, the threshold voltages of the devices modified with PMMA and PαMS were 10.72 and 15.01 V, respectively, which were also lower than those of the devices modified with PVP (42.20V) and PVA (20.22V). Moreover, the device with bare SiO_2 insulator also showed higher V_{Th} (43.25V). Because higher density of electron traps in the dielectric surfaces usually leads to increased threshold voltages, the results presented here indicate that the hydroxyl groups of the buffer polymers must associate with the presentation of electron traps. In addition, due to the completely absence of hydroxyl groups (electron traps) on the PαMS and PMMA surfaces, higher performance of n-channel conduction was observed. Therefore, in the section, the electrons trapped mechanism was compared with those of other researcher's studies.

4.6.2 Paper Review

In 2005, Chua *et al*. observed the disappearance of n-channel operation by the formation of SiO^- on the SiO_2 gate-insulator surface in inert environment.[13] They demonstrated that the use of an appropriate hydroxyl-free gate dielectric, such as a divinyltetramethylsiloxane-bis (benzocyclobutene) derivative (BCB), can yield n-channel OTFTs based on most conjugated semiconducting polymers which give the field-effect electronic mobilities in the range of 10^{-3} to 10^{-2} cm^2/Vs.
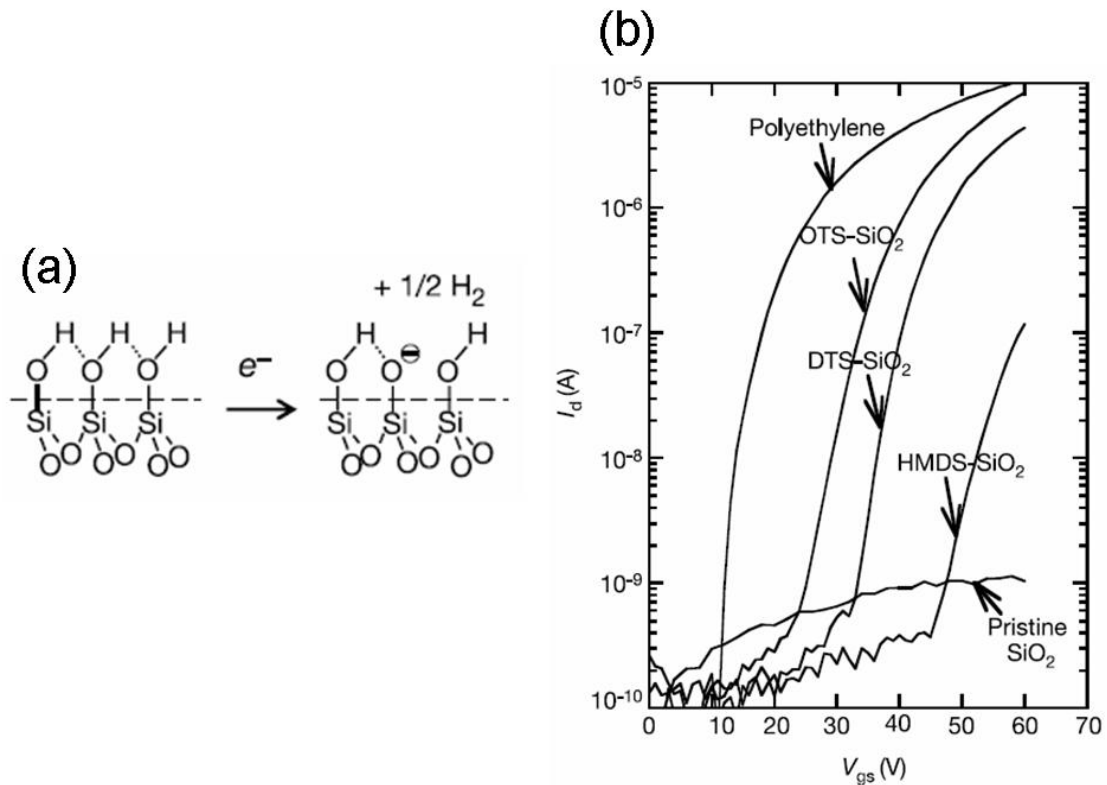
Figure 4. 12 (a) The creation of surface trap states and (b) F8BT n-channel FETs with various siloxane self-assembled monolayers (SAMs) on SiO_2 as dielectric, or with polyethylene as buffer dielectric.[13]

The electrochemical OH electron-trapping mechanism is shown in Figure 4.12 (a). The immobile negative ions, created at the interface between insulator and active layer, cause the effective threshold voltage shifting to larger value on F8BT n-type OTFTs. The silanol groups (SiOH), existing at the SiO_2 dielectric interface, definitely quench the n-channel field-effect behavior of the OTFTs. The hydroxyl-free dielectric materials can passivate the electrochemical reaction of charge carrier trapping, as shown in Figure 4.12 (b).

In addition, D. Kumaki *et al*. announced the influence of H_2O and O_2 on the device properties of OTFTs in 2008.[35] The V_{th} shift present in transfer characteristics before and after exposure to ambient air and dry air was investigated, although the mobilities in saturation region were almost unchanged in various environments [Figure 4.13]. They

indicated that the SiO^- present at the SiO_2 insulator surface, induced by the deprotonation processes of SiOH caused by H_2O and O_2, influenced the significant V_{th} shift. The electrochemical reactions are illustrated in equation 4-1 and 4-2.
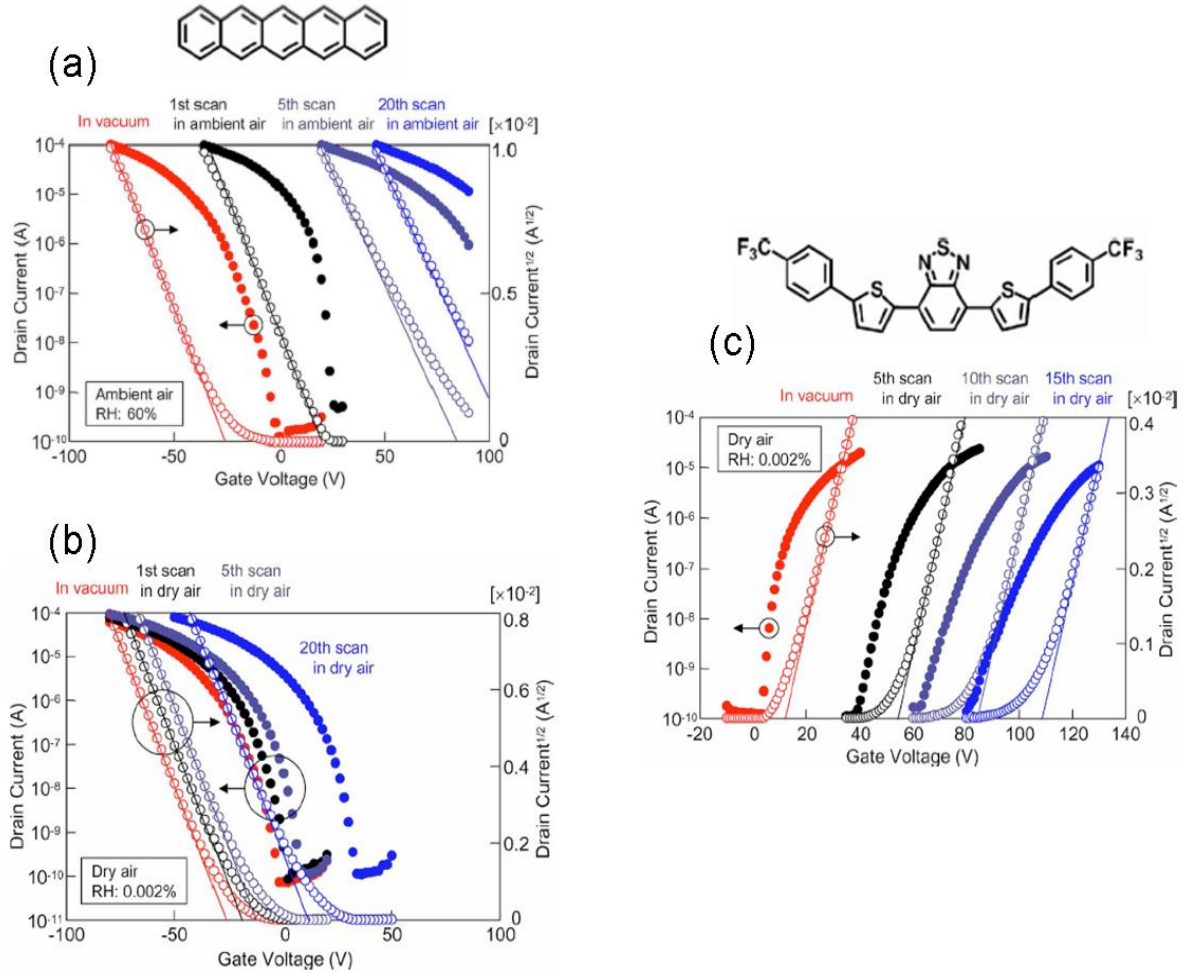
Figure 4. 13 The transfer characteristics of p-type and n-type OTFTs with threshold voltage shift in dry air or ambient air.[35] (a) and (b) are the performances of pentacene-based OTFTs measured before and after exposure to ambient air and dry air, respectively. (c) BTD-based OTFTs were measured before and after exposure to dry air.

$$SiOH + H_2O \Leftrightarrow SiO^- + H_3O^+ \qquad (4\text{-}1)$$

$$SiOH + e^- + \frac{1}{4}O_2 \rightarrow SiO^- + \frac{1}{2}H_2O \qquad (4\text{-}2)$$
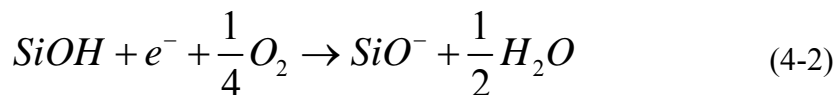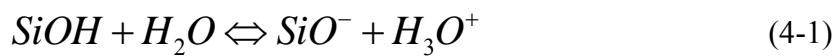
4.6.3 Mechanism

While the device performance measured under inert conditions was relative to the surface morphology and the surface energy of the dielectric layer, the electrical properties obtained under ambient environment were more sensitive to water and moisture affinity. Table 4.10 lists the water contact angle of various dielectric surfaces. The PαMS and PMMA surfaces exhibited rather hydrophobic nature, suggesting that the improved air-stability is probably associated with the moisture affinity. Recently, some researchers concluded that the adsorption of H_2O and O_2 was likely involved with an electron transfer reaction (Section 4.6.2).[35-37] In our cases, we observed clear n-channel field-effect behavior using SiO_2 as the dielectric surface while the device was measured under inert conditions [Table 4.3]. The result was different from the observation of disappearance of n-channel behavior on untreated SiO_2 surface by Chua *et al*.,[13] which was probably due to the rather insensitivity to the charging of silanol groups of PTCDI derivatives. In the contrast, the much weak n-channel field-effect behavior could be obtained while the device with bare SiO_2 insulator was measured in atmosphere. Therefore, we inferred that the hydrophobic polymers probably inhibit the approach of water to the conducting channel.

The hydrophobic property of the polymers, comparing with that of SiO_2 surface, limits of the absorption of humility, thereby retarding the degradation of n-channel behavior under ambient environment. For PVP and PVA devices, the hydroxyl groups probably have less acidities, leading to fewer tendencies to undergo the deprotonation reaction with H_2O. Therefore, the PVP and PVA devices had higher air-stability than that of the device fabricated on bare SiO_2 surfaces.

## 4.7 Other Experiments to Indicate Passivation of Surface States

In addition to the above-mentioned investigations, other experiments also performed to illustrate specifically the effects of hydroxyl groups on device performances in our work. Firstly we used various cross-linked ratios of PVP to PMCFM in order to control the density of hydroxyl groups on the dielectric layer[38]. Over and above, we modified the hydroxyl-free dielectric surface as PMMA with UV-ozone treatment to oxidize the polymer surface of OTFTs based on PTCDI-C8.

4.7.1 Various Cross-linking Ratios of PVP to PMCFM

The poly(melamine-*co*-formaldehyde) methylated [PMCFM] working as a cross-linking agent was solved in propylene glycol monomethyl ether acetate at different ratios to PVP. While the amounts of PMCFM in PVP solution were increased, more PVP molecules were cross-linked and the density of hydroxyl groups decreased.[38]

Figure 4.14 illustrates the I_d-V_d characteristics of the devices modified with PVP dielectric polymer and exhibits the poor n-channel field-effect property in the device where the ratio of PVP to PMCFM is 3:1. There was a similar outcome to the previous results and the threshold voltage shift obviously exhibited in Figure 4.15. In terms of the consequences in this experiment, the spreading of hydroxyl groups at interface provided a tendency toward the creation of the negative charge traps and resulted in the larger threshold voltages.

The strength of cross-linking effect among PVP molecules leads to the tendency to retard the electrochemical reaction with ambient air at the interface. The transfer properties demonstrate that the device with higher ratio of PMCFM to PVP has rather effective passivation from air at the dielectric surface.
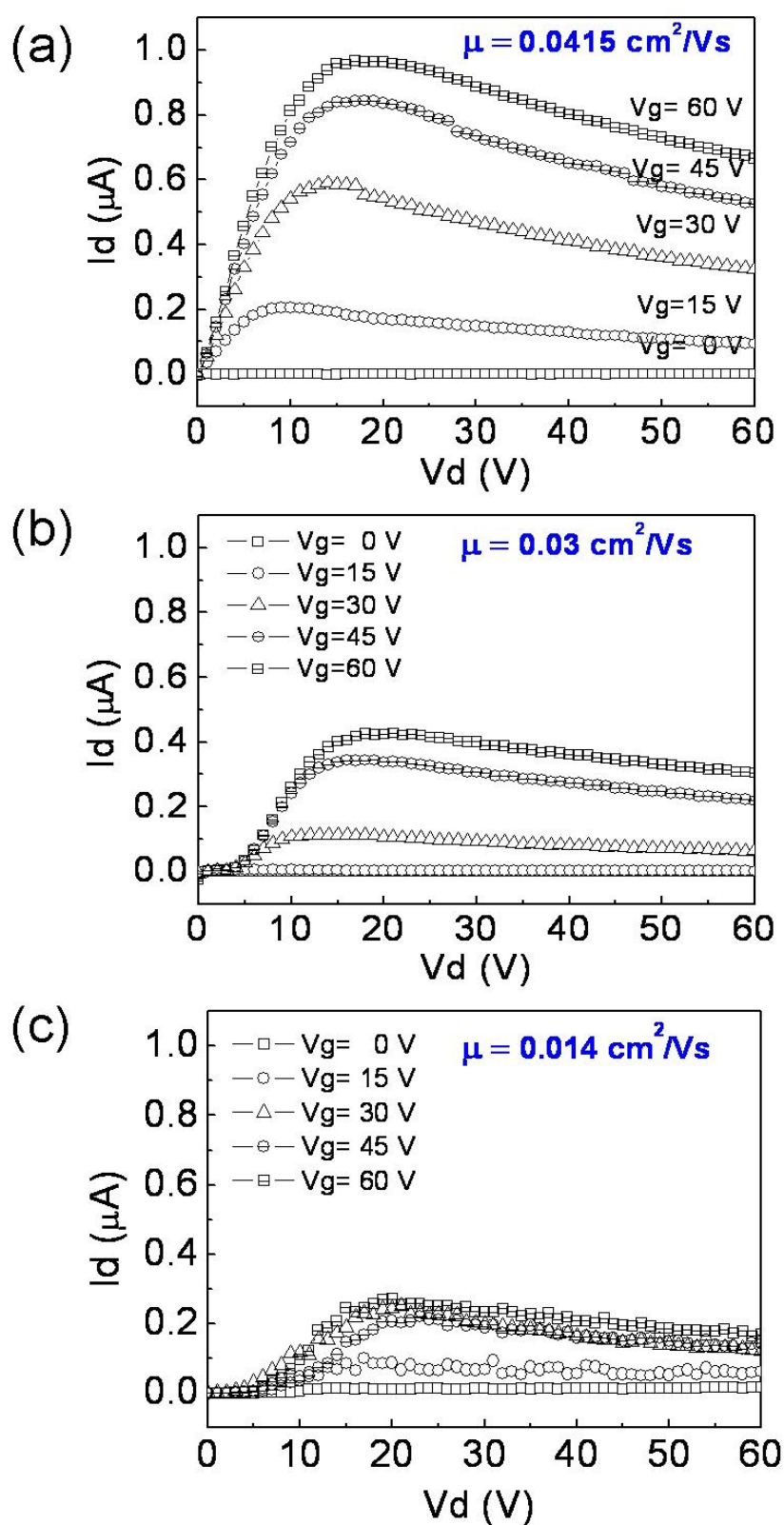
Figure 4. 14 The I_d-V_d characteristics of the devices with various cross-linking ratios of PVP to PMCFM. (a)-(c) the ratios of PVP to PMCFM are 1:1, 2:1 and 3:1, respectively.
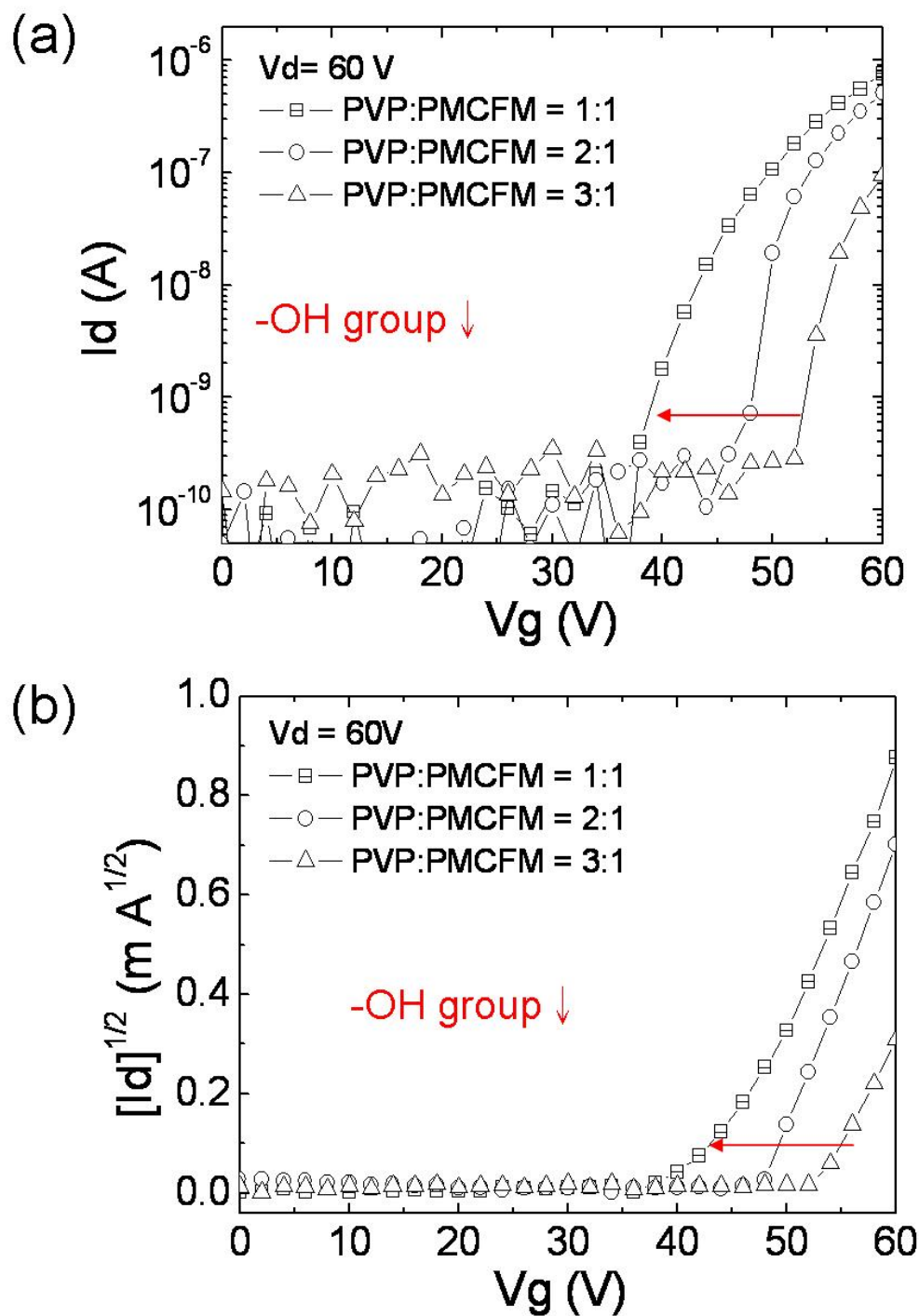
Figure 4. 15 (a) The I_d-V_g characteristics of the devices with various cross-linked ratios of PVP to PMCFM. (b) The plot of square root of drain current versus gate voltage and the electron mobilities were calculated from the slopes of that in the saturation region.

4.7.2 UV-ozone Treatment on hydroxyl-free Polymer Surface

After spin-coating hydrophobic hydroxyl-free polymer dielectrics such as PMMA and PαMS, the dielectric surfaces were treated with UV-ozone to oxidize the polymer surfaces of the OTFTs based on PTCDI-C8. The procedure of this experiment is illustrated in Figure 4.16. Subsequently, more interfacial states, such as hydroxyl groups, will be generated at the surface of the polymer buffer layer.
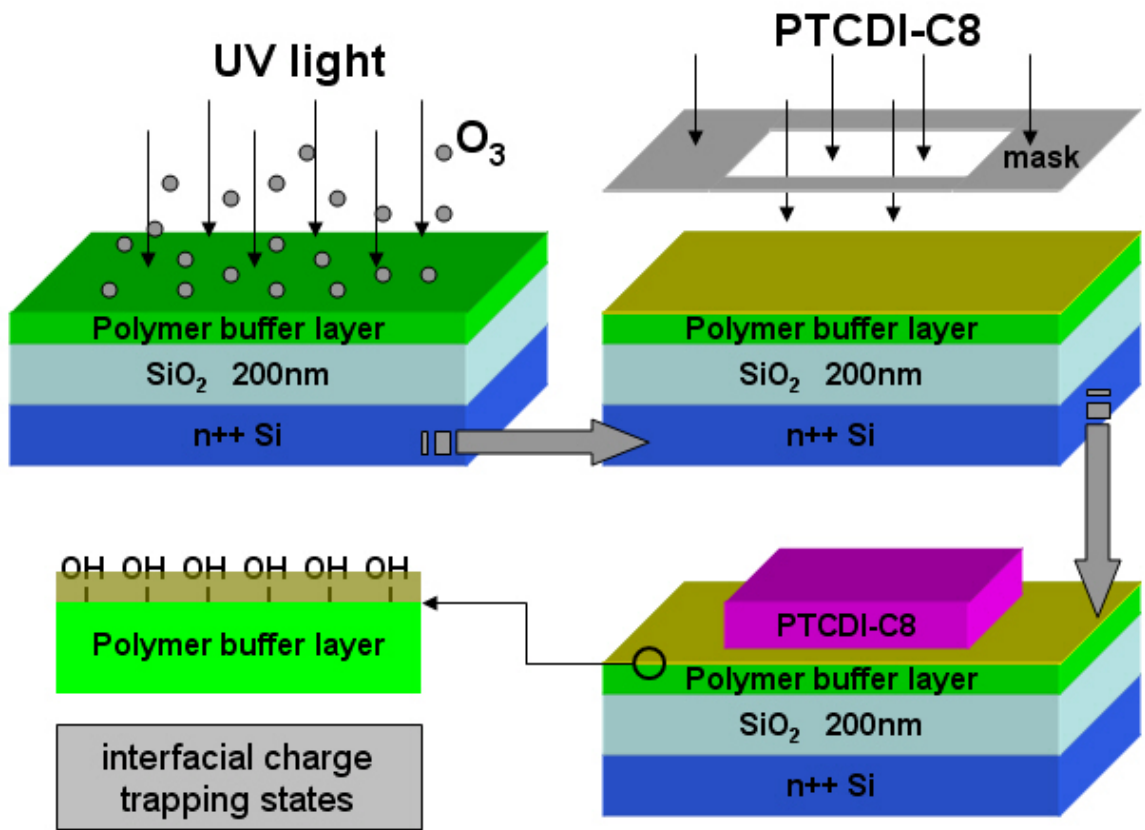
Figure 4. 16   The process of UV-ozone treatment on the hydroxyl-free polymer dielectric layer and then depositing the PTCDI-C8 on the modified layer.

The interfacial states of hydroxyl-like groups caused by oxygenation quench the n-channel field-effect characteristics, as shown in Figure 4.17. The oxidized states probably behave as surface traps. Therefore, the result here further confirms the n-channel behavior is associated with the surface states on the dielectric layer.
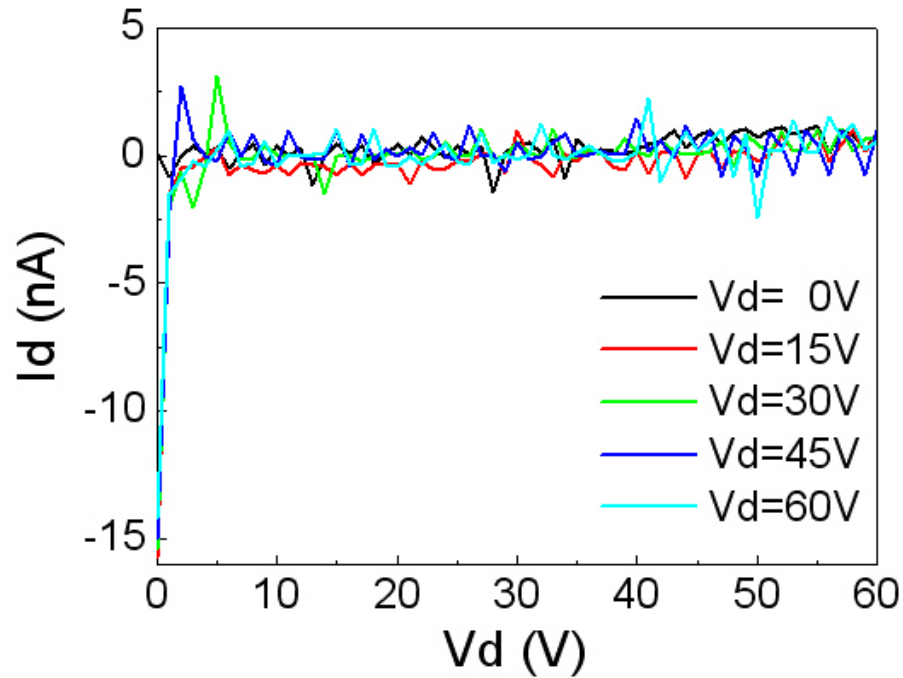
Figure 4. 17 The disappearance of n-channel behavior on the OTFTs based on PTCDI-C8 with UV-ozone treatment on the hydroxyl-free polymer dielectric layer.

4.8 Bias Stress

In this work, we also used the bias stress test to observe the threshold voltage shift in order to recognize the creation of surface trapping states. Firstly, bias stress on the device based on PTCDI-C8 with bare SiO_2 insulator at a stressed gate voltage of 40 V for 1 hour in the N_2-filled glove box, and measuring the transfer characteristics before and after bias stress, as shown in Figure 4.18. However, the slope of square root of drain current versus gate voltage was almost consistent during the V_{Th} shift, indicating that the field-effect mobility was nearly unchanged. The slightly positive shift of 3.6 V on threshold voltage is probably caused by the creation of negative surface charges (SiO^-) inducing extra positive charges in channel region of the semiconductor layer, which is similar to the conception of the report by Chua *et al*.[13]
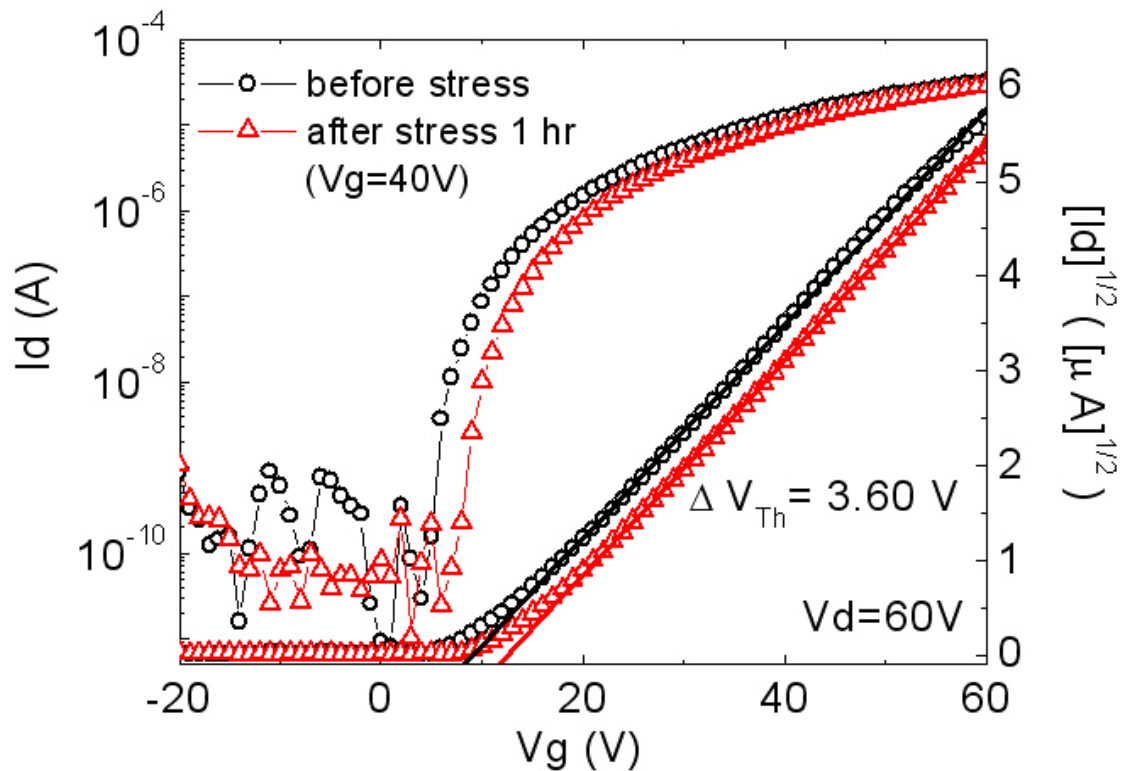
Figure 4. 18   The transfer characteristics of the device with bare SiO_2 insulator before and after bias stress at $V_g = 40$ V under inert environment. The positive threshold voltage shift is 3.6 V. The device was operated at $V_d = 60$ V.

Further, because of the relative better air-stability on PTCDI-C8 OTFT with PMMA modification upon SiO_2 insulator, that device was taken to bias-stressed at a gate bias of 40 V for 1 hour, respectively, in inert environment and ambient atmosphere. Compared with the threshold voltage shift of the bare SiO_2 case, the V_{Th} of the OTFT with PMMA modification under inert condition presents unapparent shift and almost can be ignored, such shown in Figure 4.19. The reason is that the hydroxyl-free dielectric polymer passivates the siloxyl groups (SiOH), and then fewer surface charges are induced at the interface on the device with PMMA modification by the same bias stressing at 40 V gate voltages for 1 hour.
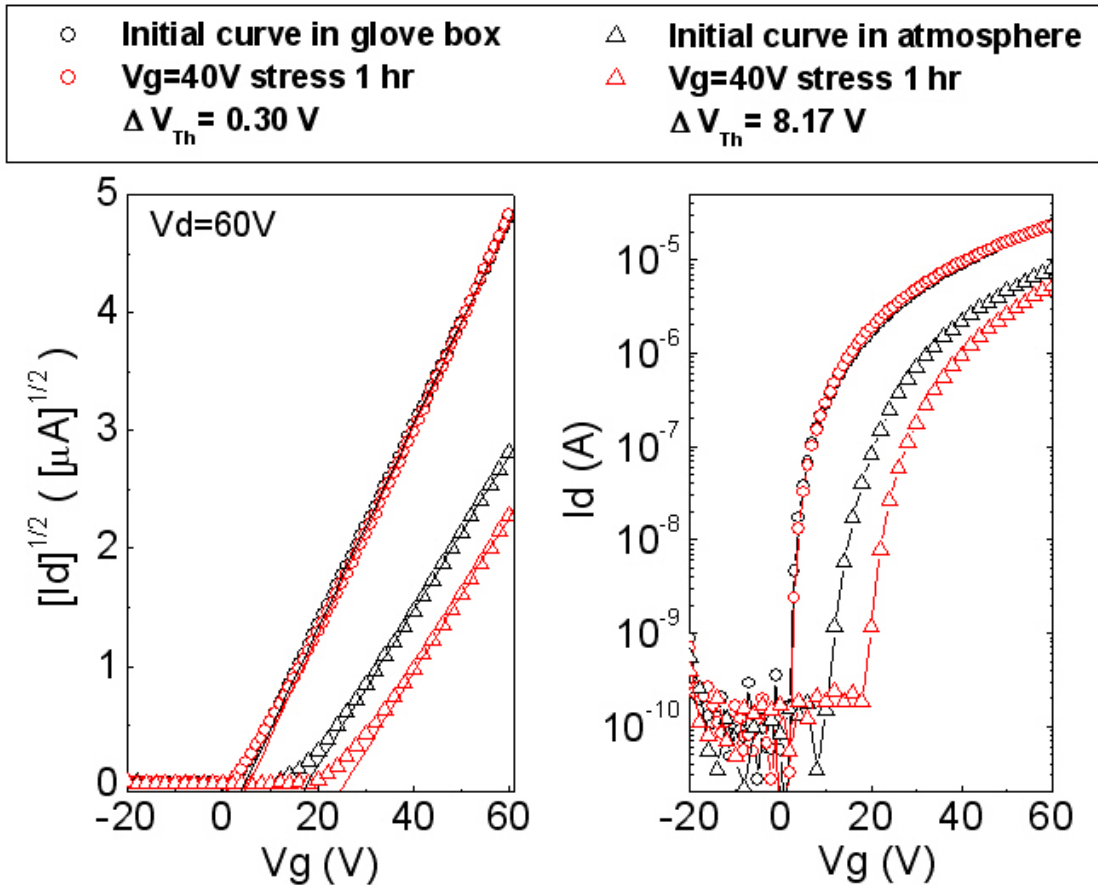
Figure 4. 19 The transfer characteristics of the device with PMMA modification upon SiO_2 insulator before and after bias stress at $V_g = 40$ V under inert environment and atmosphere. The device was operated at $V_d = 60$ V.

Figure 4.19 illustrates that the threshold voltage shift (8.17 V) in ambient atmosphere is significantly larger than that (0.30 V) in N_2-filled glove box and the slopes of square root of drain current versus gate voltage were almost consistent in both various conditions. We previously inferred that the hydrophobic polymers inhibit the approach of H_2O to the conducting channel and then the relatively air-stable OTFTs based on PTCDI-C8 can be obtained; nevertheless, H_2O is not totally suppressed out of channel region and O_2 may lead to the tendency toward the creation of electron trapping states since the obvious threshold voltage shift is obtained after exposing the transistor to air. Moreover, the influence of O_2 and additional H_2O on PTCDI-C8 OTFTs has to be taken into account.

However, the presentation of a little decay of mobility, proportional to the slope of square root of drain current versus gate voltage, after exposing device to air is most probably due to the change of the width of band tail caused by the creation of deep acceptor-like trap states[39] in the PTCDI-C8 film.

Actually, a large quantity of unidentifiable knowledge in this field of air-stability on n-type OTFTs such as PTCDI-C8 will have needed to be straightened out.

4.9 The Substrates with Various Temperatures

Finally, we especially tried out another method to concretely improve the transfer performance on the n-type OTFTs based on PTCDI-C8. The organic semiconductor was deposited on the baked substrates with modification of PMMA, and then depositing Au as source and drain electrodes defined by shadow mask at room temperature.

The field-effect mobility of the devices which has the temperature of substrates at 90℃ during depositing PTCDI-C8 could be obtained above the value of 0.4 cm^2/Vs. The higher temperatures were applied to the substrates with polymer dielectric as PMMA, and then the transfer characteristics exhibited larger electronic mobilities except for the temperature of 120℃ (Figure4.20).

The explanation can be obtained from Figure 4.21 which illustrates the morphology of 50 nm PTCDI-C8 films deposited on various substrate temperatures. The grain size of top-view of PTCDI-C8 film on the baked substrate became larger than that on the unheated substrate, and the frame of stacks of PTCDI-C8 displayed elongated lamellar grains on the baked substrate. The roughness of AFM topographies was reduced from the warmer substrate during depositing PTCDI-C8 and that led to less numbers of grain boundaries present among the PTCDI-C8 stacks. Besides, the field-effect electronic mobilities had particular improvement due to the decrease of the density of grain boundaries of PTCDI-C8 films.
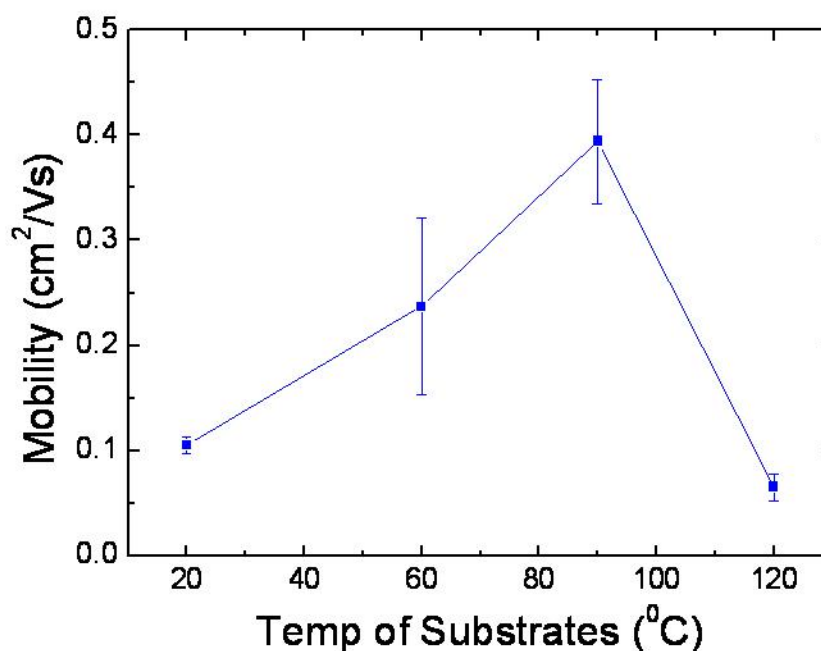
Figure 4. 20 The mobilities of devices with various temperatures of the substrates during depositing organic semiconductor as PTCDI-C8.

Even though the grin size of PTCDI-C8 at 120℃ substrate was the largest one, the field-effect performance exhibited awful electronic mobilities. The phenomenon can be attributed to that the substrate temperature of 120℃ was higher than the glass transition temperature (Tg) of PMMA which is about 110℃. The orientation of PMMA was changed after baking the substrate at 120℃ and affected the organization of the PTCDI-C8 stacks with the result that the especially hotter substrate, exceeding 110℃, with PMMA diminished the field-effect mobilities.
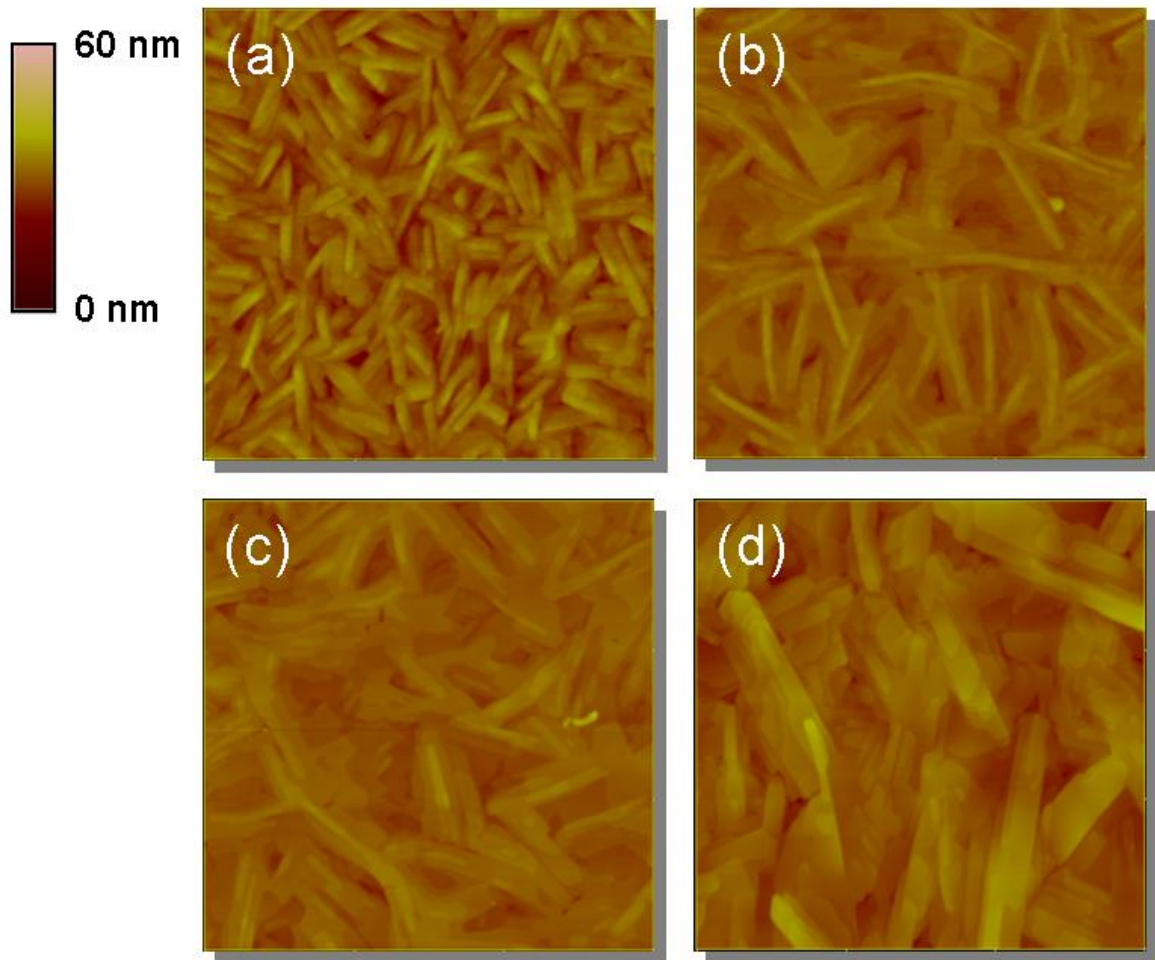
Figure 4. 21 The 3×3 μm AFM images of 50 nm PTCDI-C8 deposited on the substrates with various temperatures. (a)-(d) are indicated at 20℃, 60℃, 90℃, and 120℃, respectively.

Chapter 5
Conclusion

In conclusion, we have found that the modification of SiO$_2$ surface by hydroxyl-free polymer insulators, such as PMMA and PαMS, can improve the air-stability of n-channel OTFTs based on PTCDI-C8. The air-stability is attributed to the passivation of the siloxyl groups as electron trapping sites on the SiO$_2$ surface. In addition, the appropriate polymer dielectric surfaces like PMMA and PαMS can lead to the better crystallinity and orientation of molecules.

Furthermore, the better filed-effect characteristic can be especially obtained for the obvious made with elevated substrate temperature. The glass transition temperature (T$_g$) of dielectric materials must be taken into consideration. The results presented here were quite significant because no complicated chemical synthesis of n-channel organic materials with strong electron withdrawing groups is required.
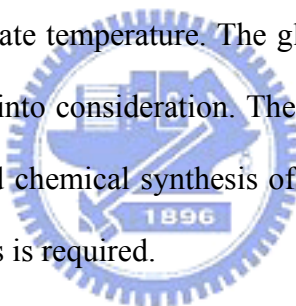
Reference

[1] R. Rotzoll, S. Mohapatra, V. Olariu, R. Wenz, M. Grigas, K. Dimmler, O. Shchekin, and A. Dodabalapur, Appl. Phys. Lett. **88**, 123502 (2006).

[2] P. F. Baude, D. A. Ender, M. A. Haase, T. W. Kelley, D. V. Muyres, and S. D. Theiss, Appl. Phys. Lett. **82**, 3964 (2003).

[3] J. A. Rogers, Z. Bao, K. Baldwin, A. Dodabalapur, B. Crone, V. R. Raju, V. Kuck, H. Katz, K. Amundson, J. Ewing, and P. Drzaic, Proc. Natl. Acad. Sci. U.S.A. **98**, 4835 (2001).

[4] H. Sirringhaus, T. Kawase, and R. H. Friend, MRS Bull. **26**, 539 (2001).

[5] G. H. Gelinck, H. E. A. Huitema, E. van Veenendaal, E. Cantatore, L. Schrijnemakers, J. van der Putten, T. C. T. Geuns, M. Beenhakkers, J. B. Giesbers, B. H. Huisman, E. J. Meijer, E. M. Benito, F. J. Touwslager, A. W. Marsman, B. J. E. van Rens, and D. M. de Leeuw, Nat. Mater. **3**, 103 (2004).

[6] L. S. Zhou, A. Wanga, S. C. Wu, J. Sun, S. Park, and T. N. Jackson, Appl. Phys. Lett. **88**, 083502 (2006).

[7] S. Lee, B. Koo, J. G. Park, H. Moon, J. Hahn, and J. M. Kim, MRS Bull. **31**, 455 (2006).

[8] M. Pope, and C.E. Swenberg, *Electronic Processes in Organic Crystals and Polymers*. (Oxford University Press, New York, 1999).

[9] J. Zaumseil, and H. Sirringhaus, Chem. Rev. **107**, 1296 (2007).

[10] H. Klauk, M. Halik, U. Zachieschang, G. Schmid, W. Radlik, and W. Weber, J. Appl. Phys. **92**, 5259 (2002).

[11] Y. Y. Lin, D. J. Gundlach, S. F. Nelson, and T. N. Jackson, IEEE Electron Devices Lett. **18**, 606 (1997).

[12] H. E. Katz, A. J. Lovinger, J. Johnson, C. Kloc, T. Siegrist, W. Li, Y. Y. Lin, and A. Dodabalapur, Nature **404**, 478 (2000).

[13] L. L. Chua, J. Zaumseil, J. F. Chang, E. C. W. Ou, P. K. H. Ho, H. Sirringhaus, and R. H. Friend, Nature **434**, 194 (2005).

[14] Z. Bao, Adv. Mat. **12**, 227 (2000).

[15] S. Tatemichi, M. Ichikawa, T. Koyama, and Y. Taniguchi, Appl. Phys. Lett. **89**, 112108 (2006).

[16] Y. Hosoi, and Y. Furukawa, Mol. Cryst. Liquid Cryst. **462**, 37 (2007).

[17] D. Kumaki, S. Ando, S. Shimono, Y. Yamashita, T. Umeda, and S. Tokito, Appl. Phys. Lett. **90**, 053506 (2007).

[18] T. D. Anthopoulos, B. Singh, N. Marjanovic, N. S. Sariciftci, A. M. Ramil, H. Sitter, M. Colle, and D. de Leeuw, Appl. Phys. Lett. **89**, 213504 (2006).

[19] Z. A. Bao, A. J. Lovinger, and J. Brown, J. Am. Chem. Soc. **120**, 207 (1998).

[20] B. Yoo, T. Jung, D. Basu, A. Dodabalapur, B. A. Jones, A. Facchetti, M. R. Wasielewski, and T. J. Marks, Appl. Phys. Lett. **88**, 082104 (2006).

[21] C. R. Newman, C. D. Frisbie, D. A. daSilvaFilho, J. L. Bredas, P. C. Ewbank, and K. R. Mann, Chem. Mater. **16**, 4436 (2004).

[22] R. Schmidt, M. M. Ling, J. H. Oh, M. Winkler, M. Könemann, Z. Bao, and F. Würthner, Adv. Mater. **19**, 3692 (2007).

[23] L. G. Kaake, Y. Zou, M. J. Panzer, C. D. Frisbie, and X. Y. Zhu, J. Am. Chem. Soc. **129**, 7824 (2007).

[24] G. Horowitz, Adv. Mater. **10**, 365 (1998).

[25] P. G. Lecomber, and W. E. Spear, Phys. Rev. Lett. **25**, 509 (1970).

[26] S. Kobayashi, T. Nishikawa, T. Takenobu, S. Mori, T. Shimoda, T. Mitani, H. Shimotani, N. Yoshimoto, S. Ogawa, and Y. Iwasa, Nat. Mater. **3**, 317 (2004).

[27] K. P. Pernstich, S. Haas, D. Oberhoff, C. Goldmann, D. J. Gundlach, B. Batlogg, A. N. Rashid, and G. Schitter, J. Appl. Phys. **96**, 6431 (2004).

[28] S. M. Sze, *Physics of Semiconductor Devices*. (Wiley, New York, 1981).

[29] G. Horowitz, F. Dellofre, F Garnier, R. Hajlaoui, M. Hmyene, and A. Yassar, Synth, Met. **54**, 435 (1993).

[30] T. Young, Philos. Trans. R. Soc. **95**, 65 (1805).

[31] Y. Hosoi, D. Tsunami, I. Hisao, and Y. Furukawa, Chem. Phys. Lett. **436**, 139 (2007).

[32] R. J. Chesterfield, J. C. McKeen, C. R. Newman, P. C. Ewbank, D. A. da Silva, J. L. Bredas, L. L. Miller, K. R. Mann, and C. D. Frisbie, J. Phys. Chem. B **108**, 19281 (2004).

[33] M. Petit, R. Hayakawa, Y. Wakayama, and T. Chikyow, Journal Of Physical Chemistry C **111**, 12747 (2007).

[34] S. Wu, *Polymer Interface and Adhesion*. (Marcel Dekker, New York, 1982).

[35] D. Kumaki, T. Umeda, and S. Tokito, Appl. Phys. Lett. **92**, 093309 (2008).

[36] R. J. Chesterfield, J. C. McKeen, C. R. Newman, C. D. Frisbie, K. R. Mann, and L. L. Miller, J. Appl. Phys. **95**, 6396 (2004).

[37] S. Ogawa, T. Naijo, Y. Kimura, H. Ishii, and M. Niwano, Appl. Phys. Lett. **86**, 252104 (2005).

[38] S. C. Lim, S. H. Kim, J. B. Koo, J. H. Lee, C. H. Ku, Y. S. Yang, and T. Zyung, Appl. Phys. Lett. **90**, 173512 (2007).

[39] C. R. Kagan, and P. Andry, *Thin-Film Transistors*. (Marcel Dekker, New York, U.S.A., 2003).